Modelling pioneer vegetation establisment at constructed salt marshes from seasons to decades

T.R. Siegersma, P.W.J.M. Willemsen, E.M. Horstman, B.W. Borsje

Abstract

Nature-based Solutions that combine salt marshes with traditional coastal protection structures are gaining popularity in the face of ongoing climate change. Vegetation establishment is of major importance herein as it facilitates salt marsh growth in lateral and vertical direction. However, the effects of marsh-supporting management measures (e.g. brushwood dams) on the establishment of pioneer vegetation on salt marshes are still understudied. To that end, this study quantifies hydrodynamic and morphodynamic thresholds for vegetation establishment based on observations from a constructed salt marsh. Bed level changes, inundation, and vegetation characteristics of the dominant pioneer species *Salicornia* were monitored during growing season 2021. Subsequently, the existing hydromorphodynamic DET-ESTMORF model was extended with the ability to predict vegetation establishment based on these thresholds. This extended model was then used to predict pioneer vegetation establishment on the short-term under different dam heights and on the long-term under expected sea level rise the coming 80 years. Increased dam height does not result in a significant increase in vegetation establishment. Sea level rise caused the vegetation boundary to retreat landward each decade until almost no vegetation was present anymore in the year 2100. The extended DET-ESTMORF model can hence be used to simulate the effects of different management measures on vegetation establishment on a constructed salt marsh.

Keywords: Nature-based Solutions, ecosystem services, DET-ESTMORF

1 Introduction

Salt marshes provide a wide range of ecosystem services (ESS). From maintaining commercial fisheries [1, 2], facilitating habitats and nursery grounds for various bird species [3], to functioning as a carbon sink [4], and as a natural buffer between the sea and coastal areas [5, 6, 7]. Salt marshes have been embanked in the past for various reasons [8, 9], on the one hand due to the intensification of agricultural activity and on the other hand due to the strong confidence in conventional coastal protection measures, like dikes, seawalls and jetties [10]. However, conventional coastal protection measures are designed at a fixed height and soil compaction or subsidence might cause these to decrease in elevation [5, 11]. On the contrary, due to their sediment-trapping ability, salt marshes are ought to - to a certain extent - keep up with sea level rise that is caused by global warming [12, 13, 14]. Therefore, in regard to the ongoing climate change, necessary costly maintenance processes on conventional designs combined with the additional benefits salt marshes can bring, could be reason to believe that nature-based solutions (NbS) integrating both conventional structures as well as salt marshes is more effective and cost-efficient than measures excluding salt marshes [15].

Consequently, salt marsh restoration and expansion projects have gained ground in Europe as well as in North America [16, 17]. Examples of management measures used to support these projects are passively abandoning all human activities and letting the natural tidal action take over to restore the pristine salt marsh communities [17] or actively facilitating restoration by the construction of sedimentation fields surrounded by (brushwood) dams [18, 19]. To improve the success rate of such restoration or expansion projects, scientists try to gain a better understanding of the factors that are important in salt marsh development [7].

Natural salt marshes usually originate where increased volumes of sediment are deposited along a sheltered intertidal area, leading to higher topographic elevation. In case of constructed salt marshes, management measures like anthropogenic sand nourishment and/or the implementation of (brushwood) dams facilitate this initial phase of salt marsh development [18]. Previous research has shown that artificial structures are successful in the field in increasing salt marsh width [20] by attenuating wave height and thereby increasing sedimentation rates [21]. As a result, the area landward of the dam becomes more suitable for colonization by pioneer vegetation [22]. Besides sedimentation and erosion resulting in vertical motion of the salt marsh, they also develop in a lateral direction. Lateral expansion is driven by seedling establishment and subsequent growth of pioneer vegetation, whereas landward retreat is caused by erosion due to storms and waves [23], or forced by the formation of cliffs, occurring when the marsh extends too far seawards [21].

The challenge of predicting the development of the initial phase of NbS lies in the fact that mechanisms that facilitate and quantify the establishment of pioneer vegetation influenced by implemented management measures have not been studied sufficiently [24]. Necessary physical, biological and chemical conditions should be met for successful settlement of pioneer vegetation propagules. Accordingly, an inundation-free period of a certain time span is necessary for young seedlings to settle [24], and bed level dynamics should not be too extreme in or-

der to prevent uprooting or burial of the seedlings [25, 26]. The magnitude of erosion or sedimentation processes is in turn influenced by the soil composition: a high mud/sand ratio results in higher erosion rates than in a soil with a lower mud/sand ratio, because cohesive forces play a smaller role [27].

Improved understanding of the effects of bed level dynamics, inundation time and implemented management measures on the vegetation establishment on salt marshes will contribute to the success rate of NbS on the short and the long term. To that end, this study investigates the following research question *'What are the effects of protective structures and climate change-driven sea level rise on the establishment of pioneer vegetation on Nature-based Solutions?'*. This study combines newly obtained monitoring data on the establishment of salt marsh pioneer vegetation with a state-of-the-art dynamic equilibrium theory model for morphological salt marsh development. By monitoring vegetation growth and environmental factors on a constructed salt marsh during growing season, relations between inundation, bed level change and vegetation establishment were scrutinised. The physically-based hydromorphodynamic DET-ESTMORF model was elaborated with the resulting relations from the field in order to make well-justified predictions about the establishment and subsequent growth of pioneer vegetation (Methods). Such models yet exist (e.g. Delft3D), but are very time- and computer power-consuming, whereas this elaborated model works very quick and efficient. Furthermore, the extended DET-ESTMORF model offers the novel possibility to explore the effects of management measures on the NbS, such as the implementation of brushwood dams or the elevation of the bathymetry with sand nourishment. Therefore, the model was used to predict short- and long-term vegetation establishment as a result of implemented management measures (Results). This study was concluded with an evaluation of the found results and implications on forthcoming Nature-based Solution-projects (Discussion).

2 Methods

2.1 Field site

The Marconi salt marsh constructed in Delfzijl (northern part of the Netherlands) is a typical example of a Nature-based Solution still in its establishing phase, and was therefore selected as site for field measurements [28]. The salt marsh was constructed in 2017 and the overall bed level was increased with sand nourishment. Marconi covers up 15 ha and its area is divided into six sections separated by brushwood dams, which are also used to reduce stress and to increase the sediment accretion. Different volumes of mud and sand were mixed with the nourished sand, thereby constructing sections with soil types containing different percentages of mud (5%, 20% and 50%) (Figure 1). On the landward side of the salt marsh, the sections are enclosed by a dike. The Mean High Water level in the estuarine environment near Delfzijl is 1.40 m above Dutch Ordnance Datum (NAP) and the mean semi-diurnal meso-tidal range covers 3.06 m [29].

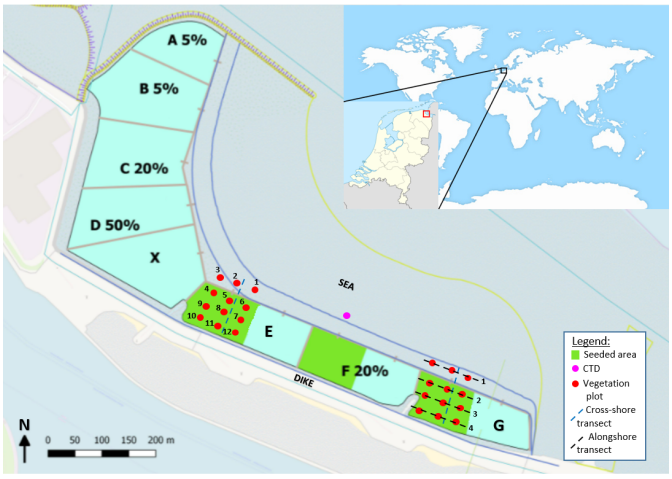

Figure 1: *Graphical representation of Marconi salt marsh [28] with locations of vegetation plots (red dots) and CTD-sensor (pink dot). The dotted lines are enumerated and indicate the locations of the alongshore (black) and cross-shore transects (dark blue). The enumeration of the vegetation plots in section E was applied to section G in a similar way.*

The dominant pioneer species on the developing Marconi salt marsh are the *Salicornia procumbens* and *Salicornia europeana* (hereafter both referred to as *Salicornia* as they are of the same genus) (Figure 2). Their growing season spans from April/May to August/September. Half of the sections E, F, and G were seeded in 2017 with fragments of *Salicornia procumbens* (Figure 1).

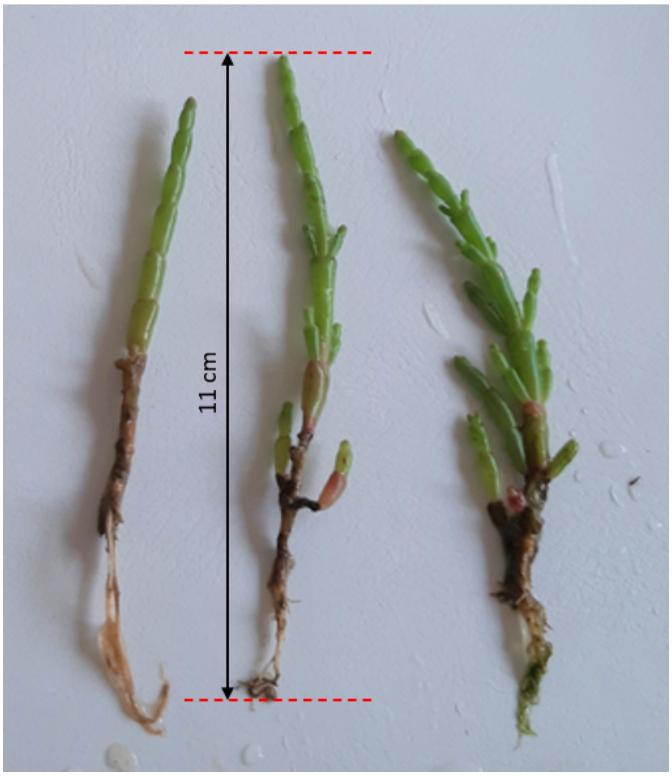

Figure 2: *Specimens of Salicornia: the dominant pioneer species on Marconi. These particular vegetation units were collected from the field during the field trip the 1st of July 2021.*

2.2 Data collection and processing

Nine vegetation plots (0.5x0.5 m, Figure 3) demarcated with erosion pins were located alongside three alongshore transects within the brushwood dams in the seeded areas of both sections E and G and three plots alongside an alongshore transect outside the brushwood dams (Figure 1). Sections E (50%) and G (5%) were chosen as measurement sites to include the largest difference between the soil conditions, i.e. mud percentage, but to keep the rest of the environmental conditions constant. A gradient of hydrodynamic exposure of the plots was accounted for as the vegetation plots were located in each section on four alongshore transects that varied in cross-shore distance (with transect 1 being most seaward located and transect 4 closest to the dike).

Figure 3: *Measurement set-up of the vegetation plots (0.5 x 0.5 m) on the Marconi salt marsh. The erosion pins mark the two diagonal corners of the vegetation plot for consistency of the measurements over the growing season. Every field trip, the erosion pins were measured, five Salicornia plants in the vicinity of each vegetation plot were analysed, and a photo was taken from above the vegetation plot to determine the FVC.*

The vegetation plots were used to monitor vegetation characteristics of *Salicornia* (Figure 2) and to measure bed level change processes. A Conductivity, Temperature and Depth measuring device (CTD) was stationed just outside section F (Figure 1) to measure local water depth. The field observations were made on monthly or bi-monthly basis (Table 1): the installation of the measurement instruments was done on the 23th of April 2021 and the subsequent measurements were executed on the 2nd of June, 1st of July, 30th of July and the 28th of September 2021.

2.2.1 Vegetation growth

Five individual *Salicornia* specimen surrounding the vegetation plots (Figure 3) were collected from the soil every field trip. Then the shoot length, root length, longest root length, diameter of widest part of the shoot, and the weight of the whole unit and of the shoot were measured after roughly removing the largest sand particles (Appendix A). The values for root length, shoot length and weight of the five units per vegetation plot were averaged for a monthly distinct value of the vegetation characteristics per plot.

Additionally, the fractional vegetation cover (FVC) was approximated based on pixel analysis of photos taken from a distance of circa 1.5 m above each vegetation plot [30]. Image segmentation in vegetation and background was done by pixel classification. Each pixel contains color information saved as values for red, green and blue (RGB). Mathematical operations with these color values can accentuate certain pixel characteristics, captured in an index value. Logically, the color green is of large interest to detect pixels containing vegetation.

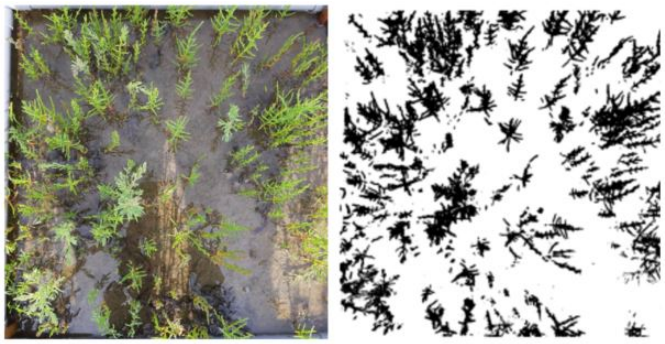

Figure 4: *Conversion of photograph taken from a vegetation plot (left) to a black-and-white picture distinguishing the vegetation (black pixels) from the background pixels (right) using the index value ExGR. This particular photograph is a snapshot from vegetation plot G9 (Figure 1) the 30th of July and resulted in a value for the FVC of 24.8%.*

To come to a value for FVC per vegetation plot, the images were first cropped to display only the vegetation plot and were then compressed to 1000 x 1000 pixels in consideration of computational efficiency. Next, for each pixel in the compressed photograph the values for *Excess Green* and *Excess Red* were calculated with Equation 1 and 2 respectively [30], which together made up for the index value *Excess Green minus Excess Red (ExGR = ExG - ExR)*. All pixels with a value lower than 0 for this index were categorised as being vegetation, whereas pixels with higher values were considered as background pixels (c.f. Meyer, 2008 [31]), and the resulting ratio represents the FVC per vegetation plot (Figure 4). In some cases green algal mats covering the entire vegetation plot

Table 1: *Overview of different field measurements and corresponding frequencies. The measuring devices were installed in the field on the 23th of April 2021 and following measurements were executed on the 2nd of June, 1st of July, 30th of July and the 28th of September 2021.*

Variable	Interval or continuous	Number of measurements
Bed level change	Monthly or bi-monthly	Two measurements per vegetation plot
Shoot length	Monthly or bi-monthly	Five measurements per vegetation plot
Root length	Monthly or bi-monthly	Five measurements per vegetation plot
Biomass	Monthly or bi-monthly	Five measurements per vegetation plot
Density	Monthly or bi-monthly	One photo per vegetation plot
Inundation	Once every 5 minutes during high tide	One central measurement point
Bed level elevation	Once the first month	One cross-shore transect per section

made it impossible to distinguish between vegetation and background. Then an estimate for the FVC was made based on a visual comparison with photographs showing a similar vegetation cover for which the FVC had been computed automatically.

$$ExG = 2G - R - B \tag{1}$$

$$ExR = 1.4R - G \tag{2}$$

2.2.2 Erosion and sedimentation

Each vegetation plot was marked with two erosion pins (duplicates) in two diagonal corners (Figure 3) (c.f. Willemsen, 2018 [26]). Erosion pins consisted of bamboo sticks of approximately 1 cm in diameter that were pushed at least half a meter deep into the bed to ensure that wave action did not pull them from the soil. Every field trip the above-ground length of the erosion pins was monitored by lowering an erosion disk (diameter 10 cm) over the pin and measuring the distance from the top of the pin to give insight in the monthly bed level dynamics in each vegetation plot. This erosion disk was used to ensure unambiguous measurements and to correct for possible scouring holes that arose around the erosion pins.

To determine the monthly bed level change per vegetation plot, the length of the erosion pin measured in the current month was subtracted from the length in the preceding month. This gives a positive value when sedimentation has occurred and a negative value for erosion. The resulting bed level change per vegetation plot was obtained by averaging the corresponding two duplicates (Figure 3).

2.2.3 Inundation

The CTD-sensor in front of the seeded area of section F (Figure 1) was used to measure the local water depth (c.f. Van Regteren, 2019 [32]). The device measured with a frequency of once every five minutes. However, the device ran out of memory at the start of September, so the inundation for the last month of the growing season was determined based on water level data monitored by the *Dutch Department of Waterways and Public Works* (RWS). The water level in m + NAP was measured at the German measurement station *Knock* and obtained from the RWS database. This station was chosen because it was located closest to Delfzijl without any objects and structures obstructing free flow, hence making the tidal characteristics similar [33].

The water depth measured in the field during high tide with the CTD device was converted to water level data by adding the bed level elevation of the CTD device location (0.4 m + NAP) and the height of the CTD head above the bed (0.1 m). The water level data was used to obtain the monthly inundation percentage per vegetation plot by determining what fraction of the total passed time the water level was higher than the bed level at the respective vegetation plots. The assumption was made that there was no slope in the water level across the salt marsh and that there were no obstructions on the salt marsh preventing the water level from reaching higher elevated vegetation plots.

2.2.4 Bed level elevation

During the installation day of the measurement instruments (April, 23), the cross-shore bed level elevation was measured relative to NAP with a Differential Global Positioning Sensor *(DGPS GNSS Leica C 15)* in the two sections E and G. Measurements were taken with an interval of 2 m along the cross-shore transect that intersects the middle row of vegetation plots (Figure 1). Furthermore, the bed level elevation at each separate erosion pin was measured with the DGPS device.

2.2.5 Biophysical relations for vegetation growth

As a first exploratory study of the data set, the monthly inundation percentage and bottom level change per vegetation plot were analysed. Then, a distinction was made between the plots containing vegetation and bare plots (vegetated and unvegetated plots) and thresholds for inundation and bed level change were identified. This way, areas that were suitable for vegetation presence (environmental conditions stay between or below thresholds) were distinguished from areas that were not suitable (environmental conditions exceed thresholds).

Once it was determined where vegetation can exist, the development of the growth was of interest. The difference in vegetation growth between the two sections E and G with different sediment composition was examined by comparing the average

values of the vegetation characteristics (root length and shoot length) between the sections. A two tailed t-test was conducted to assess whether the characteristics of vegetation in the two sections were significantly different. Eventually, relations between the months passed and the shoot and root length were determined in order to derive a parameterisation of the aboveground and belowground length of the vegetation over time. These relations were obtained with logistic regression, as vegetation growth is generally described by a logistic function [34].

2.3 Model set up

For the purpose of predicting vegetation establishment on a Nature-based Solution, the dynamic equilibrium theory (DET)-ESTMORF model was used as it provides a simple and sufficient tool to simulate tidal bed level changes that have an effect on the establishment of vegetation [35, 36, 37, 38]. The model describes the morphological dynamics based on both physical processes (hydrodynamics and sediment transport) as well as morphological equilibrium relations (Figure 5).

The model requires input values with a 20 minute interval for significant wave height (H_s) and peak wave period (T_p) at the seaward boundary and water level data during high tide, as the model only simulates during high tide (Figure 5). Consequently, it was assumed that no morphodynamic changes occur during low tide. The DET-ESTMORF model is calibrated to the bed level dynamics measured in section E, because dynamics in section G could not be reproduced for several reasons described in the Discussion. Hence, the initial bathymetry of section E should be defined to simulate the bed level changes as a result of tidal forcing.

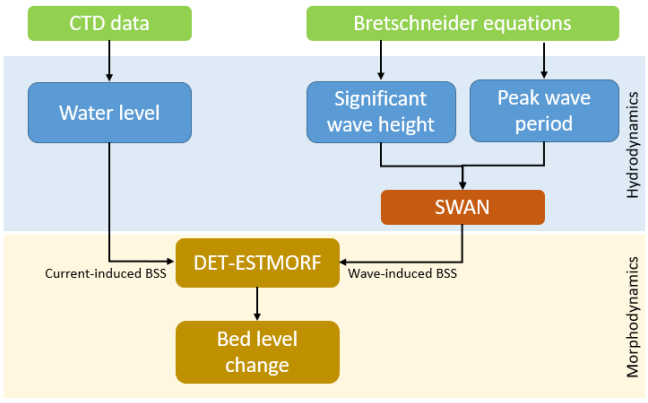

Figure 5: *Overview of the DET-ESTMORF model structure, that consists of a morphodynamic and hydrodynamic component.*

2.3.1 Morphodynamics

The main idea behind the model is the assumption that sediment is only transported in suspension. Consequently, there exists an idealized state in which the morphological system is in equilibrium with uniform overall bed shear stress (BSS) τ_E. In this state, the vertical erosion flux compensates for the vertical sedimentation flux, hence no net sedimentation or erosion

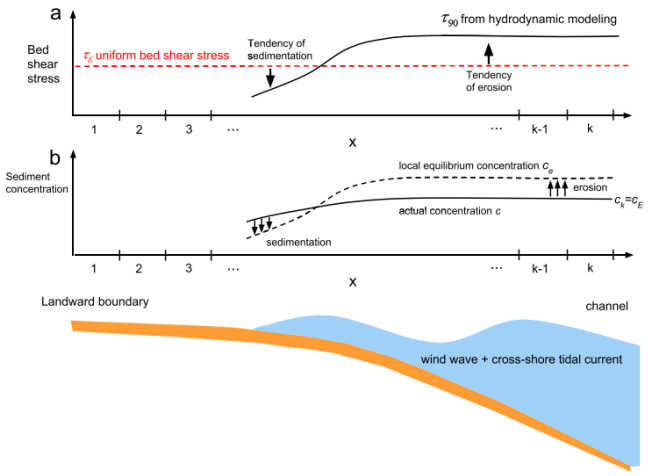

Figure 6: *Schematic overview of the DET-ESTMORF model [36]. The 1D cross-shore model domain consists of k grid cells and stretches from the landward (x=0) towards the seaward boundary (x=k). Above: when the local BSS (τ_{90}) in grid cell x deviates from the uniform overall BSS (τ_E), a tendency for either sedimentation or erosion exist in grid cell x. Below: the ratio between τ_{90} and τ_E determines the local equilibrium sediment concentration c_e, while the actual sediment concentration field c is governed by a diffusion equation. The eventual difference between c and c_e determines the actual net morphodynamic change at the end of each high tide.*

occurs in the system. Therefore, the overall prevailing equilibrium sediment concentration c_E is defined according to Equation 3 [39, 40].

$$m_e\left(\frac{\tau_E}{\tau_{cr}} - 1\right) = c_E w_s \tag{3}$$

where m_e is the erosion coefficient (kg/m^2/s) (Table 2), τ_{cr} the critical BSS for erosion (Pa) and w_s the settling velocity for suspended sediment (m/s). Consider a cross-shore transect consisting of grid cells, ranging from grid cell 1 most landward to grid cell k most seaward (Figure 6). According to the concept and formulation in the original ESTMORF models, the local equilibrium concentration in each grid cell (c_e) is dependent on the ratio between the local BSS (τ_{90}) and the overall equilibrium BSS (τ_E) as represented in Equation 4 [41, 37].

$$c_e = c_E\left(\frac{\tau_{90}}{\tau_E}\right)^n \tag{4}$$

where τ_{90} is the 90th percentile bed shear stress in a tidal cycle (Pa) and n is the power for the local equilibrium sediment concentration. If the local BSS in a grid cell is lower than the equilibrium bed shear stress ($\tau_{90} < \tau_E$), the bed is inclined towards sedimentation in this grid cell and c_e is lower than c_E. Conversely, in case the local BSS is higher than the equilibrium BSS ($\tau_{90} > \tau_E$), the grid cell has a preference towards erosion and c_e is higher than c_E.

However, whether the morphological change of corresponding preference really happens in the grid cell depends on the actual sediment availability, governed by a diffusion equa-

tion as described in Equation 5.

$$\frac{\partial(hc)}{\partial t} = w_s(c_e - c) + \frac{\partial}{\partial x}(Dh\frac{\partial c}{\partial x}) \quad (5)$$

where h is the water depth during high water (m), t is time (s), x the cross-shore distance from the seaward boundary (m), c the sediment concentration by volume (m^3/m^3) and D is the tide-averaged diffusion coefficient (m^2/s) (Table 2). When a grid cell is inclined to erode based on the difference between c_e and c_E, but the actual available sediment concentration (c) is high enough to prevent this from happening, erosion may not occur.

In summary, the difference between τ_E and τ_e determines the inclination of a grid cell towards morphological change. This inclination is expressed in terms of a single representative value per grid cell per tidal cycle for the local equilibrium sediment concentration (c_e). Morphological change only occurs when the actual sediment concentration (c) is different from the local equilibrium sediment concentration (c_e): erosion takes place when c is smaller than c_e, whereas sedimentation takes place when c is lager than c_e. After each tidal cycle, the actual bed level change is determined according to Equation 6.

$$\frac{\partial z}{\partial t} = \frac{1}{1-p} w_s(c - c_e) \quad (6)$$

where z is the bed level (m) and p is the soil porosity (-) (Table 2).

Table 2: *Important DET-ESTMORF model parameters, used values and sources.*

Parameter	Value	Source
ρ_s (kg/m^3)	2650	[42]
ρ_w (kg/m^3)	1024	-
m_e (kg/m^2 s)	0.00005	[43]
f_c (-)	0.002	[43]
D (m^2/s)	30	[35]
p (-)	0.4	[44]
ν (m^2/s)	0.000001	-

2.3.2 Hydrodynamics

The hydrodynamic forcing of one tidal cycle is expressed in terms of the 90th percentile bed shear stress (Equation 4), because it includes both the magnitude of the forcing as well as the fraction of time the forcing is strong. The local values for τ_{90} arise from tidal currents and wave action. The cross-shore current (u_c) evolves from water volume conservation in tides' quasi-static propagation [45, 46, 47]. With rising tide, the water line moves gradually landward over the salt marsh. The volume of water (ΔV) that must pass through a vertical plane parallel to the shore at grid cell x is equal to the increase of the water volume landward from this grid cell. The cross-shore current at this grid cell over a time interval of (Δt) can then be determined with Equation 7.

$$u_c(x,t) = \frac{\Delta V(x,t)}{\Delta t h(x,t) B} \quad (7)$$

where B is the unit alongshore width of the grid cells (-). The resulting current-induced bed shear stress (τ_{cur}) is calculated with Equation 8.

$$\tau_{cur} = \rho_w f_c u_c^2 \quad (8)$$

where ρ_w is the density of water (kg/m^3) and f_c a constant friction factor for currents (-) (Table 2).

For the quantification of the wave action, the 1-D spectral wave model SWAN (Simulating WAves Nearshore) [48] is forced by the Joint North Sea Wave Project wave field [49] on the model domain boundary. Default values were used for parameters involved in the simulation of the wave dispersion. The generated values for certain wave characteristics by the SWAN model were used for the quantification of the wave-induced bed shear stress (τ_w) according to Equation 9

$$\tau_w = 0.5 \rho f_w u_{wave}^2 \quad (9)$$

where u_{wave} is the root-mean-square value of the maximum orbital motion near the bed, which is part of the SWAN output and f_w is a friction factor (-) that is estimated by Equation 10.

$$f_w = 1.39(\frac{\xi}{k_s/30})^{-0.52} \quad (10)$$

where k_s is the Nikuradse roughness length: 2.5$\cdot$ D_{50}, with D_{50} representing the mean grain diameter of the surface sediment (m) and ξ the particle excursion amplitude (m) close to the bed, which can be deduced from the SWAN output. The mean bed shear stress results from the combined influence of currents and waves during a tidal cycle as described in Equation 11 [50].

$$\tau_m = \tau_{cur}\left[1 + 1.2(\frac{\tau_w}{\tau_{cur}+\tau_w})^{3.2}\right] \quad (11)$$

And the maximum bed shear stress during a wave cycle can be calculated with Equation 12.

$$\tau_{max} = \left[(\tau_m + \tau_w|cos\theta_\alpha|)^2 + (\tau_w|sin\theta_\alpha|)^2\right]^{0.5} \quad (12)$$

where θ_α is the angle (°) between the direction of the current and wave propagation, which can be regarded as zero (θ_α=*0* °), since it was assumed that both are in cross shore direction close to the coast. The 90th percentile of τ_{max} was eventually used as BSS input for the determination of the local equilibrium sediment concentration in Equation 4.

2.3.3 Initial conditions

Important model parameters and corresponding values are listed in Table 2 and a complete overview can be found in Appendix B. The initial bathymetry for section E was constructed with the bed level elevation data collected in the field from the cross-shore transect during the installation day. The bed level elevation was measured approximately every 2 m along the transect, so the graph connecting these points was smoothed to prevent sharp edges from occurring in the bathymetry. For modelling purposes, the smoothed bathymetry was extended

with a typical gradient for the Dutch Westerschelde estuary that was previously used for salt marsh modelling with DET-ESTMORF [36]. The resulting cross-shore transect was divided into grid cells of 1 m length.

The constructed bed level profile from section E ranges from an elevation of 2.0 m to -2.0 m + NAP (Figure 7) and the grid consists of 279 cells of 1 m length. The increase in the bed level at approximately 100 m distance from the landward boundary can be explained by the formation of a sand bank. The brushwood dam is located at a distance of 93 m from the landward boundary and has a height of 0.4 m above the bed. Furthermore, the fluctuations in the bed level landward of the dam can partly be ascribed to a heavy track-laying vehicle that was used during the construction of the salt marsh in 2017 leaving behind tire tracks [28].

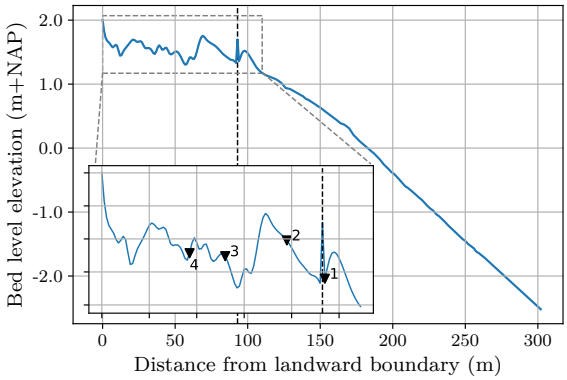

Figure 7: *Initial bathymetry from section E. The box in the plot shows the locations of the four alongshore transects as shown in Figure 1. The dotted black line represents the location of the brushwood dam, located 93 m from the landward boundary. Transect 1 is located 1 m seaward of the dam and transect 2, 3 and 4 are located respectively 78, 52 and 37 m from the landward boundary.*

2.3.4 Boundary conditions

The sediment concentration at the seaward boundary (c_k, Figure 6) was considered as a time-invariant boundary condition with fixed value (c_k=c_E) under the assumption that the world outside the salt marsh is always in equilibrium and that its morphology does not influence the sediment availability. The mean annual suspended sediment in the estuarine environment of Marconi is 50 mg/L [51], thus the value for the time-invariant seaward boundary was set to 0.05 kg/m^3. As a dike at the landward boundary prevents the sediment from moving further inland, the sediment flux at this boundary was set to zero. Therefore the sediment concentration at the most landward grid cell was equal to the neighbouring grid cell (c_1=c_2).

The water level is gathered from the processed data from the field and the RWS database. Since the CTD device was located at a bottom level of 0.4 m + NAP and the head was elevated 0.1 m above the ground, the measured water level data starts at a value of 0.5 m + NAP (Figure 8). Because only the morphodynamic changes occurring on the higher elevated area landward of the CTD device are of interest, the model simulates exclusively when the water level is higher than 0.5 m + NAP. The measured water level data has a mean value of 1.02 m + NAP, whereas the maximum water level reached an elevation of 2.13 m + NAP (Figure 8). The latter two peaks show the water level retrieved from the RWS database and these are in the same order of magnitude as the prior peaks determined with the CTD data (Figure 8).

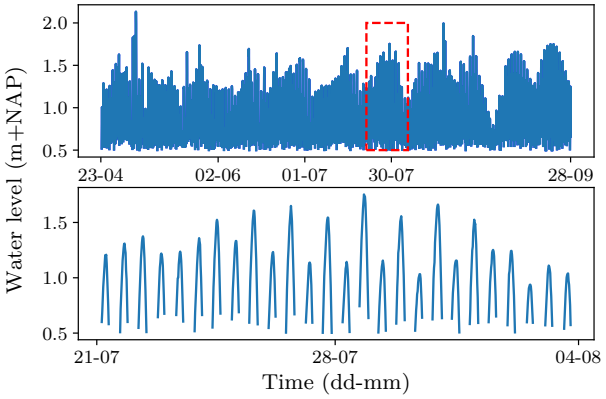

Figure 8: *Water levels used as input for the DET-ESTMORF model to simulate growing season 2021 (above. The mean water level is 1.02 m + NAP and the maximum reached during this period is 2.13 m + NAP. The red box indicates the water levels that are zoomed in on (below) in the period between 21st of July and 4th of August for clarification purpose.*

The significant wave height (H_s) and peak wave period (T_p) were obtained with the use of Bretschneider equations (Equations 13 to 16) [52, 53].

$$\overline{H} = 0.283 \tanh(0.532\overline{d}^{0.75}) \tanh\left[\frac{0.0125\overline{F}^{0.42}}{\tanh\left(0.53\overline{d}^{0.75}\right)}\right] \quad (13)$$

$$\overline{T} = 2.4\pi \tanh(0.833\overline{d}^{0.375}) \tanh\left[\frac{0.077\overline{F}^{0.25}}{\tanh\left(0.833\overline{d}^{0.375}\right)}\right] \quad (14)$$

$$\overline{d} = \frac{dg}{u^2}, \quad \overline{F} = \frac{Fg}{u^2} \quad (15)$$

$$\overline{H} = \frac{H_s g}{u^2}, \quad \overline{T} = \frac{T_s g}{u} \quad (16)$$

where g is the gravitational acceleration (9.81 m/s^2), T_s the significant wave period (s), u the wind speed at 10 m height (m/s), d the water depth (m) and F the fetch length (m). The water depth (d) was determined by calculating the difference between the water level and the bed level elevation of the seaward boundary. The hourly wind velocity and direction data during the growing season of interest were collected from the *Royal Netherlands Meteorological Institute* database (KNMI), measured at the weather station located at Nieuw-Beerta (closest to Delfzijl). Bretschneider requires wind velocities at 10 m height

and since this station measures wind near the ground, the values were converted according to Equation 17 [54].

$$\frac{u(z_1)}{u(z_2)} = \frac{ln(z_1/z_0)}{ln(z_2/z_0)} \tag{17}$$

where $u(z_1)$ and $u(z_2)$ are the wind velocities at height z_1 and z_2 respectively. Wind waves solely develop when the wind blows in an onshore direction. This implied for the case of Marconi that only wind blowing from the direction of 320°N to 100°N creates onshore waves, which can be approximated as northwestern and eastern wind respectively (considering the north to be 360 °and east 90 °). This particular wind-wave-generating domain was cut up in bins of 10 °, and for each bin the fetch length was determined with Google Maps© satellite imagery from 2021 (Appendix C). This resulted in fetch lengths ranging from 3.5 km to 40 km (Table 3). The fetch lengths are compensated for the location of the seaward boundary at a distance of 279 m from the dike. The significant wave period T_s was converted to the peak wave period T_p by multiplying it with a factor 1.08 [53].

Table 3: *Fetch lengths for different wind directions used for the calculation of peak wave period and significant wave height with Bretschneider equations.*

Wind direction (°)	Fetch length (km)
10	40.3
20	7.8
30	4.3
40	3.8
50	3.8
60	3.5
70	4.6
80	7.2
90	24.3
100	17.7
320	7.2
330	11.9
340	32.1
350	35.0
360 (or 0)	38.5

Bretschneider was only used when the wind was blowing in the range 320 to 100 °(Appendix C). When the wind blew outside this range, a minimum value for H_s and T_p of 0.031 m and 0.76 s respectively was assumed to simulate small waves generated locally. These numbers were the minimum values resulting from the Bretschneider equations with the smallest fetch length and wind speed as input. The resulting values for H_s range from 0.031 to 0.71 m, with an average value of 0.13 m and a standard deviation of 0.13 m, whereas the T_p fluctuates between 0.76 and 3.73 s with a mean value of 1.69 and standard deviation of 0.48 s (Figure 9).

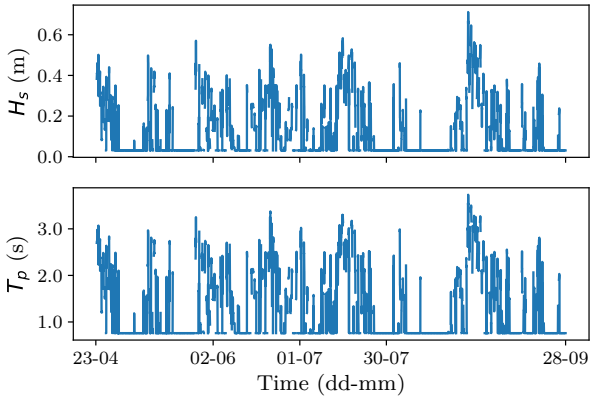

Figure 9: *Values for significant wave height (above) and peak wave period (below) resulting from Bretschneider calculations. The average significant wave height is 0.13 m and the average peak wave period is 1.69 s.*

2.3.5 Protective structures

The Marconi salt marsh was designed with the implementation of a protective brushwood dam, hence why the model should simulate the effect of this brushwood dam accordingly. The dam was modelled to have an attenuating effect only on the wave-induced BSS as the contribution of the current-induced bed shear stress to the total bed shear stress was generally a factor 1000 smaller (due to low tidal currents resulting from the rising and falling tide). Even more so, this slow flow does not experience a great deal of friction due to a semi-permeable dam as the flow finds its way through the dam. To simulate this brushwood dam the bed level elevation of one grid cell was temporarily increased to dam height just before SWAN calculates the wave-induced bed shear stress (Figure 10). After the calculation of the bed shear stress, the grid cell was converted back to the original elevation. This grid cell was also subjected to morphodynamic changes caused by the tide. The location of this elevated grid cell was chosen to have the same distance from the landward boundary as the brushwood dam has from the dike on the Marconi salt marsh.

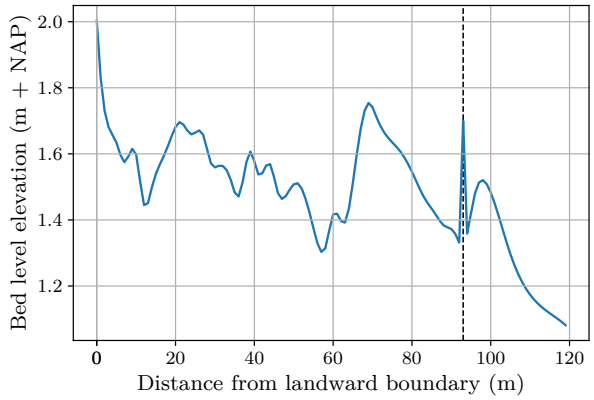

Figure 10: *Graphical representation of implementation of the brushwood dam in the bathymetry by temporary increasing the bed level elevation up to a height of 1.7 m+NAP before calculation of the wave-induced bed shear stress.*

2.3.6 Vegetation dynamics

Salt marsh vegetation establishment and growth is affected by hydrodynamic and morphodynamic forcing: propagules require a sufficiently long inundation-free period after dispersal in order to anchor successfully [24] and bed level changes should not be too high to prevent uprooting or burial of the specimen [25]. These limiting thresholds were quantified based on field measurements and were then used to implement vegetation establishment in the DET-ESTMORF model.

As erosion and sedimentation processes should not be too large, the bed level change δz_{veg} should not increase the sedimentation δz_{max} and erosion boundary $-\delta z_{min}$ for successful vegetation establishment (Equation 18).

$$-\delta z_{min} < \delta z_{veg} < \delta z_{max} \tag{18}$$

The hydrodynamic threshold was expressed as the monthly inundation percentage, as the inundation-free period plays a large role in vegetation establishment. Vegetation will not be able to settle when the monthly inundation percentage χ_{veg} exceeds the boundary value χ_{max} (Equation 19).

$$\chi_{veg} < \chi_{max} \tag{19}$$

The DET-ESTMORF model generates output in terms of bed level change (Equation 6), so the sedimentation and erosion boundaries were implemented directly into the model. The monthly inundation percentage was calculated from the water level input during high tide and the bed level elevation of each grid cell along the cross-shore transect. When the monthly bed level change in a grid cell exceeds δz_{max} or -δz_{min} or the monthly inundation percentage exceeds χ_{max}, the grid cell was marked as not suitable for vegetation establishment and no vegetation grows subsequently. The growth of the vegetation was expressed in shoot and root length and growth relations were determined with logistic regression [34] of the field measurements (Equation 20).

$$f(t) = \frac{c}{1 + ae^{-bt}} \tag{20}$$

where *a,b and c* determine the shape of the growth function.

2.4 Calibration

The calibration and validation of bed level changes simulated by the DET-ESTMORF model was previously done for a similar study site by Hu et al.[36], with a general conclusion that the overall model performance is good.

Parameters in the DET-ESTMORF model that characterise sediment were used for the calibration of the model: mean sediment grain diameter (D_{50}), settling velocity (w_s) and critical shear stress for erosion (τ_{cr}). The influence of the mean grain diameter is reflected in the model in the value for the Nikuradse roughness length ($k_s = 2.5 \cdot D_{50}$). This parameter determines the friction factor involved in the calculation of the wave-induced bed shear stress. Next, the settling velocity plays a role in the model in determining the value for the equilibrium bed shear stress (Equation 3) and in quantifying the actual bed level change (Equation 5). Finally, the critical bed shear stress for erosion determines when erosion occurs. In the model τ_{cr} is, like w_s, involved in the calculation for equilibrium bed shear stress (Equation 3).

Previous research has indicated that the prevailing mean grain sediment size in the upper 40 cm of section E varies in a range between 2 to 105 μm [28]. Therefore, for D_{50} a range of 10 to 100 μm with increments of 10 μm was used for the calibration. The settling velocity and critical shear stress were computed according to Equation 21 and 22 respectively [55].

$$w_s = \frac{(s-1)gD_{50}^2}{18\nu} \tag{21}$$

$$\tau_{cr} = \theta(\rho_s - \rho)gD_{50} \tag{22}$$

where ν is de kinematic viscosity of water (m^2/s), s the density ratio between sediment and water (2.65), ρ_s is the density of sediment and ρ the density of water (kg/m^3) (Table 2). A value for the Shields parameter θ was found with Equation 23 and 24 [55].

$$D* = D_{50}\left(\frac{(s-1)g}{\nu^2}\right)^{\frac{1}{3}} \tag{23}$$

$$\theta = 0.115D*^{-0.5} \tag{24}$$

where $D*$ is the dimensionless grain size diameter. Varying the input of D_{50} in a range of 10 to 100 μm results in a range of input values for the settling velocity and the critical shear stress for erosion (Table 4).

Table 4: *Values for the mean grain diameter, settling velocity and critical shear stress for erosion used for the sensitivity analysis and calibration purposes.*

D_{50} (μm)	w_s (m/s)	τ_{cr} (Pa)
10	0.000089	0.037
20	0.00036	0.052
30	0.00081	0.064
40	0.00144	0.074
50	0.00225	0.083
60	0.00324	0.091
70	0.00441	0.098
80	0.00576	0.105
90	0.00728	0.111
100	0.00899	0.117

For the calibration of the DET-ESTMORF model, it was assessed which values for the sediment characteristic parameters (Table 4) minimised the root-mean-square deviations of the bed level change (RMSD) (Equation 25).

$$RMSD = \sqrt{\frac{\sum(\Psi_{model} - \Psi_{obs})^2}{N}} \tag{25}$$

where Ψ_{model} is the simulated bed level change (m), Ψ_{obs} the observed bed level change (m), and N is the total number of

data points. The simulated bed level was obtained by forcing the DET-ESTMORF model with the water level, significant wave height and peak wave period data collected from the field during growing season 2021. The observed bed level change data points are the averages of the measured bed level change of each transect (Figure 1) after each month (or two months) during growing season.

2.5 Validation and sensitivity analysis

The validation of the vegetation establishment was done by comparing the modelled vegetation boundary under the conditions of growing season 2021 with the actual vegetation boundary on the Marconi salt marsh that is retrieved from a photograph from the Marconi area taken from above in the year 2020 (Figure 11).

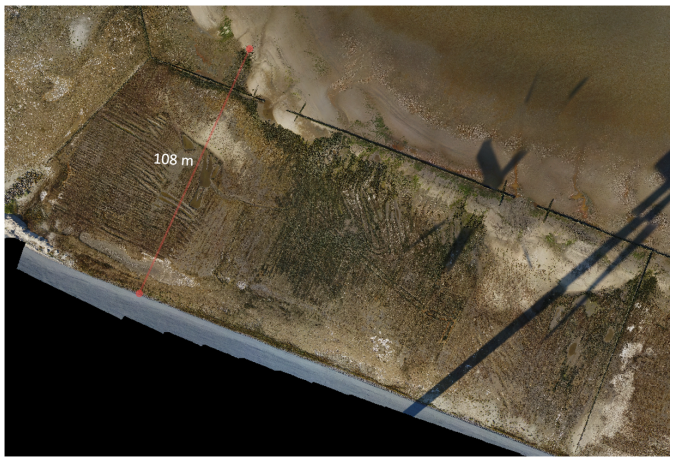

Figure 11: *Photograph taken from section E in September, 2020. The red line indicates where the pioneer vegetation was growing, hence the vegetation boundary is located at a distance of 108 m from the dike.*

To explore the influence of the three aforementioned sediment parameters on the bed level change, a sensitivity analysis was conducted with the parameter settings that correspond to a range of 10 to 100 μm for D_{50} with increments of 10 μm (Table 4).

2.6 Scenario analysis

The calibrated DET-ESTMORF model was used to assess pioneer vegetation occurrence on salt marshes under different circumstances. First it was of interest whether the height of the protective structures on Marconi has varying effects on the short-term establishment of pioneer vegetation. Hence, one growing season (from May till September) of the *Salicornia* pioneer vegetation was simulated with different reasonable dam heights ranging from 0 (no dam) to 1.6 m above the bed with increments of 0.2 m (*dam height scenario*). However, the foot of the dam is established at a relatively high bottom level elevation of 1.33 m + NAP, because of the nourishment in 2017. Since the average measured high water level during the growing season of 2021 has a value of 1.02 m + NAP, the water level only exceeds the bed level at the foot of the dam 14.4% of the total inundation time. To assess the effect of the brushwood dam height under different circumstances, the measured water level in 2021 was increased to a water level taking 40 years and 80 years of sea level rise into account (29.6 and 60 cm higher respectively, [56]). Consequently, the water exceeds the level at the foot of the dam 48% and 81% respectively of the total inundation time. Hence, besides the water level measured in 2021, the increased water level input values were used to simulate one growing season in the years 2021, 2060 and 2100 on the Marconi salt marsh with different aforementioned dam heights.

In addition, the question whether salt marshes will keep up with sea level rise has been examined in numerous studies, with a general consensus that salt marshes only thrive under the conditions that sediment deposition and biomass accumulation balance the sea level rise and seaward erosion must be compensated by landward marsh expansion [57, 58]. Sea level rise will result in higher inundation frequency of the salt marsh. Therefore, a second scenario was used to explore how the long-term establishment of pioneer vegetation on the bathymetry of the Marconi salt marsh will evolve during the coming 80 years. Simulating 80 annual growing seasons was too time-consuming, so the bed level changes and resulting vegetation establishment were instantaneously modelled with increments of decades. The global sea level rise rate under the intermediate greenhouse gas emissions scenario is estimated to be 7.6 mm/year [56], hence water levels used as forcing in the DET-ESTMORF model were increased with a value of 76 mm each decade *(sea level rise scenario)*. To assess the effect of management measures taken in 2017 to construct the Marconi salt marsh (nourishment and brushwood dam), this sea level rise scenario was also applied to the bathymetry of the area before the construction works, obtained from the Dutch Elevation database (Figure 12).

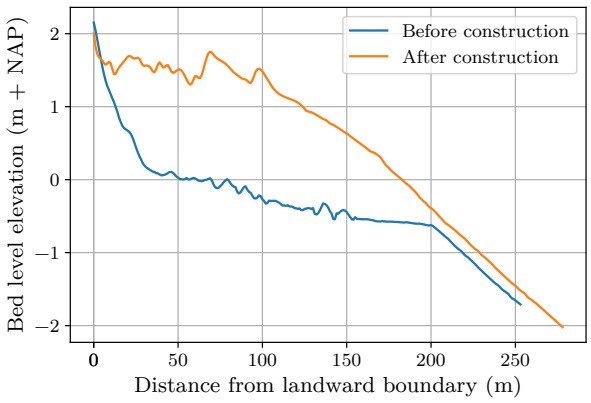

Figure 12: *Bathymetry of section E before (blue) and after (orange) the construction works in 2017.*

3 Results

3.1 Field observations

Bed level dynamics in section G were generally higher than in section E: the largest measured and average values for bed level change during growing season in section G were -7.5 cm and -0.25 cm and in section E 1.25 cm and 0.15 cm respectively (Figure 13). Furthermore, the bed seaward of the brushwood dam in section G (transect 1) showed exclusively erosion on a monthly scale during growing season, which can be explained by the fact that the bed (0.84 m+NAP) is elevated approximately half a meter lower than the bed seaward of the dam in section E (1.32 m+NAP). This also explains why the inundation percentage in transects 1 and 2 is generally higher in section G than in section E (Figure 13).

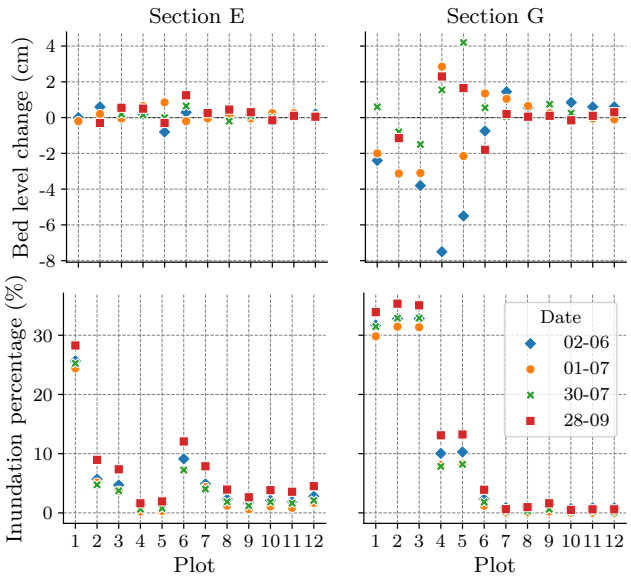

Figure 13: *Above: bed level dynamics measured once or twice a month in section E and G. The bed level change data points were constituted by the average values derived from two erosion pins per vegetation plot each month (Appendix D). Below: monthly inundation percentages of each plot in section E and G. The values were determined with the bed level elevation of these plots and the water level data. Plot numbers correspond to vegetation plot locations as shown in Figure 1.*

3.1.1 Vegetation establishment

Whether or not vegetation establishes can be explained by the local inundation percentage and bed level dynamics not exceeding the morphodynamic and hydrodynamic thresholds δz_{max}, δz_{min} and χ_{max} (Figure 14). The values for these thresholds were determined from field measurements: areas that have a higher monthly inundation percentage than 12% or higher bed level dynamics than 1.4 cm of sedimentation or 0.8 cm of erosion were found not suitable for vegetation establishment (Figure 14).

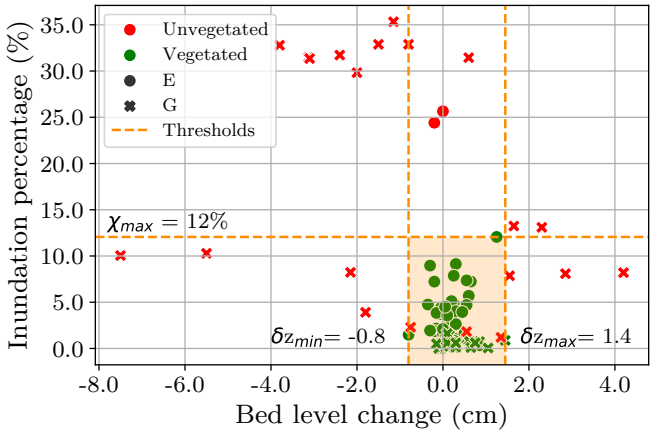

Figure 14: *Distinction between vegetated (green) and bare (red) vegetation plots with corresponding monthly bed level change (x-axis) and inundation percentage (y-axis). The orange shaded area indicates the local conditions under which vegetation can establish and the orange dotted lines represent the boundaries of these local conditions.*

3.1.2 Vegetation growth

After successful establishment of vegetation follows growth. The average vegetation density during growing season in section G was smaller than in section E (Table 5). From the measured vegetation characteristics in sections E and G, it appeared that the shoot length doesn't differ statistically between the two sections (p = *0.80*), whereas the root length of the vegetation growing in section E was systematically and significantly smaller than in section G (p = *2.51e-12*) (Figure 15).

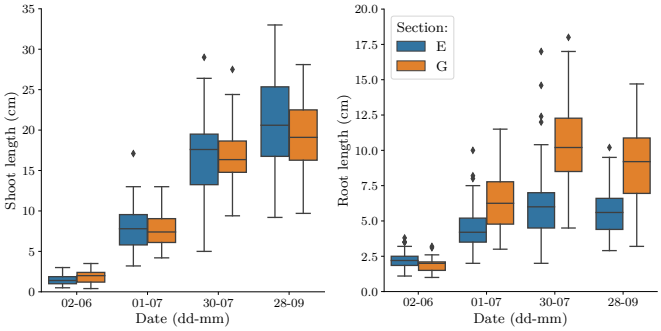

Figure 15: *Boxplots of vegetation characteristics shoot length (left) and root length (right) measured in the field. The orange boxplots represent section G, while the blue ones represent section E. The black diamonds show the measured outliers.*

Two separate growth curves for the root length were established for section E and G using logistic regression, because this vegetation characteristic was significantly different between the two sections (Figure 16). Hence, the root length can be estimated after each month (*May = 0*) for both separate sections since the start of the growing season according to:

$$Root\ length\ E = \frac{6.0}{1 + 16.9e^{-2.1 * month}}$$

$$Root\ length\ G = \frac{9.9}{1 + 56.1e^{-2.4 * month}}$$

Table 5: *Mean values and standard deviations (μ (σ)) of measured shoot length, root length, and FVC values. The values for root and shoot length are determined by averaging over all plants measured in sections E or G (Appendix E). The FVC values are obtained by calculating the average over all vegetation plots in both separate sections (Appendix F). FVC values for the field trip in September were not reliable due to the Salicornia specimens already degrading and becoming red.*

	Section E			Section G		
Date	**Shoot (cm)**	**Root (cm)**	**FVC (%)**	**Shoot (cm)**	**Root (cm)**	**FVC (%)**
02-06	1.52 *(0.67)*	2.23 *(0.64)*	1.74 *(1.66)*	1.81 *(0.78)*	1.98 *(0.51)*	0.48 *(0.46)*
01-07	7.82 *(2.83)*	4.6 *(1.59)*	8.48 *(6.42)*	7.76 *(2.26)*	6.37 *(1.99)*	5.26 *(3.38)*
30-07	16.65 *(4.93)*	6.25 *(2.61)*	16.49 *(20)*	16.64 *(3.71)*	10.25 *(2.98)*	9.37 *(6.90)*
28-09	20.82 *(5.7)*	5.71 *(1.8)*	-	19.3 *(4.69)*	9.08 *(2.95)*	-

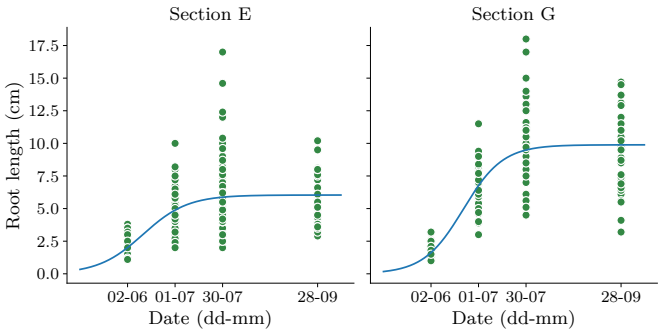

Figure 16: *Relation between root length and passing time in months of roots in section E (left) and section G (right) retrieved by logistic regression. The green dots display the spread of the measured root lengths each field trip.*

Because the shoot length does not differ statistically between the two sections, one growth curve for the shoot length was formulated by logistic regression (Figure 17). Hence, the shoot length in both sections is governed by the following growth equation:

$$Shoot\ length = \frac{20.4}{1 + 86.0e^{-2.0 * month}}$$

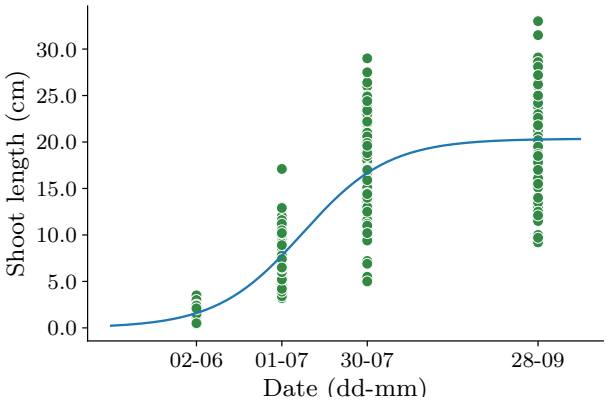

Figure 17: *Relation between length of shoots in both sections and passing time in months retrieved by logistic regression. The blue dots illustrate the spread of the collected values for shoot length each field trip.*

3.2 DET-ESTMORF

3.2.1 Calibration

Bed level changes modelled by DET-ESTMORF were calibrated to morphodynamics measured in the field on four alongshore transects in section E (Figure 7) during four field excursions. Using the parameter settings that correspond to a mean sediment diameter of 30 μm (Table 4) resulted in the minimum value for the RMSD of 0.34 cm (Figure 18).

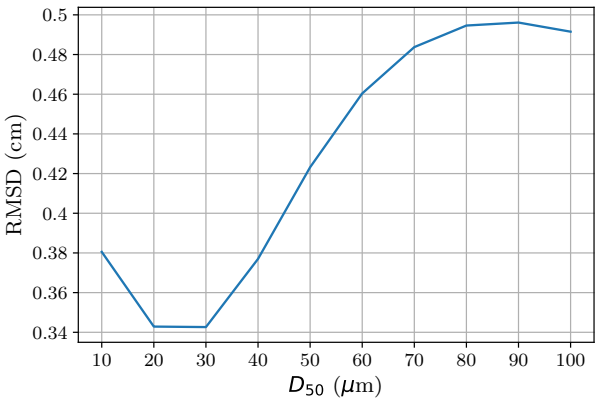

Figure 18: *RMSD values (Equation 25) that correspond to different parameter settings (Table 4). The minimum value for RMSD on section G is 0.34 cm achieved with a D_{50} of 30 μm, w_s of 0.00081 m/s and τ_{cr} of 0.064 Pa.*

Modelled cumulative bed level changes with parameter settings that correspond to D_{50} being 30 μm were largest at the two most seaward located transects 1 and 2 (Figure 19). In general, the modelled results only showed accretion of the bed, whereas in the field some erosion was measured in transects 1 and 2. Furthermore, the bed level higher up the salt marsh at transects 3 and 4 did not change much, since the water level did not reach these locations often during high tide. This is reflected in both the modelled and the measured cumulative bed level changes in transect 3 and 4 (Figure 19).

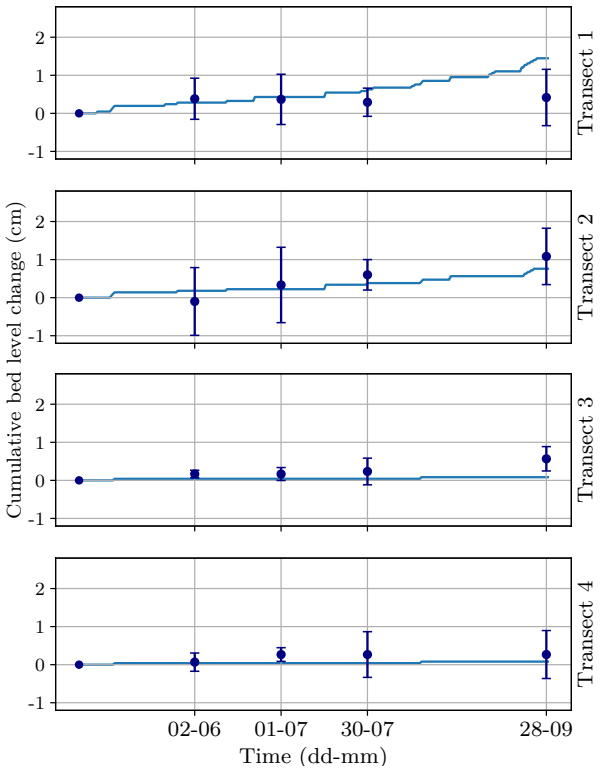

Figure 19: *Modelled (blue line) and measured (blue dots) cumulative bed level changes during the growth period along the four transects (Figure 7). The error bars show the standard deviation from the field measurements.*

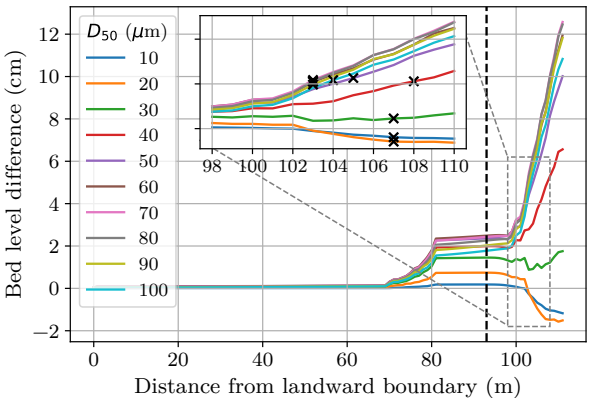

Figure 20: *Difference between the initial bathymetry (Figure 7) and the bed level after the simulated growing season 2021. Positive values mean that accretion has occurred, while negative values represent erosive action. The dotted black line shows the location of the brushwood dam. The box shows the zoomed-in differences between 98 and 110 m from the landward boundary. The black markers represent the location of the vegetation boundary after the simulated growing season 2021 for each corresponding set of sediment characteristics.*

3.2.2 Validation and sensitivity analysis

Modelling parameter settings corresponding to a mean sediment diameter of 30 μm (Table 4) on the Marconi salt marsh resulted in a vegetation boundary that is located at 107 m from the landward boundary during growing season 2021 (Figure 20). The actual vegetation boundary in the year 2020 was located at a distance of 108 m from the landward boundary (Figure 11), so the prediction of the location of vegetation boundary was really accurate. Higher accretion rates as a result of increased sediment size, critical shear stress, and settling velocity generally result in small shift of the vegetation boundary toward the landward boundary (Figure 20), because the monthly sedimentation threshold was exceeded in more grid cells.

Increasing the average sediment diameter from a value of 10 to 100 μm with corresponding values for critical shear stress and settling velocity (Table 4) led to increased sedimentation seaward of the brushwood dam (Figure 20). Larger sediment sizes correspond to faster settling velocities, which explains the increased accretion processes at the seaward side of the salt marsh. The tidal flow and wave action were apparently not high enough to maintain the sediment suspended in the water column and therefore a large part deposits. However, the differences between the sediment sizes became smaller when moving landwards of the dam, because the water level did not reach that elevation very often during high tide.

3.3 Scenario analysis

3.3.1 Dam height scenario

This scenario assessed the influence of the dam height on the vegetation boundary simulated during one growing season in the year 2021, 2060 and 2100 taking a sea level rise rate into account resulting from the intermediate greenhouse gas scenario [56]. In the growing season of 2021, the vegetation boundary under all different dam heights was located at 107 m from the landward boundary (Figure 23 *lowest bar*), whereas in the year 2100 different dam heights resulted in a vegetation boundary that was located 1 m from the landward boundary (Figure 23 *highest bar*). For the year 2060, there were small differences between the vegetation boundary location for different dam heights. When no dam was implemented in the model domain, the vegetation spread to 79 m from the landward boundary. However, increasing the dam height results in the vegetation boundary slightly moving toward the sea, until a dam height of 0.8 m (Figure 21). The reason for this movement of the vegetation boundary is that the sedimentation is higher for higher dams, resulting in increased bed levels. This causes the hydrodynamic threshold χ_{max} to be exceeded at increased distance from the landward boundary in case of higher dams.

The dam height makes no to a very small difference in the location of the vegetation boundary in one growing season in the years 2021, 2060 and 2100. However, the effect on morphodynamic changes are more apparent (Figure 22, showing bed level changes in the year 2060. The dynamics in the years 2021 and 2100 are more or less the same, but with different magnitudes). On the landward side of the dam, the bed level changes during one growing season show that higher dams result in higher sedimentation rates up to a dam height of 0.8 m. The net sedimentation in the area landward of the dam confirms that increasing the dam height above 0.8 m does not make a

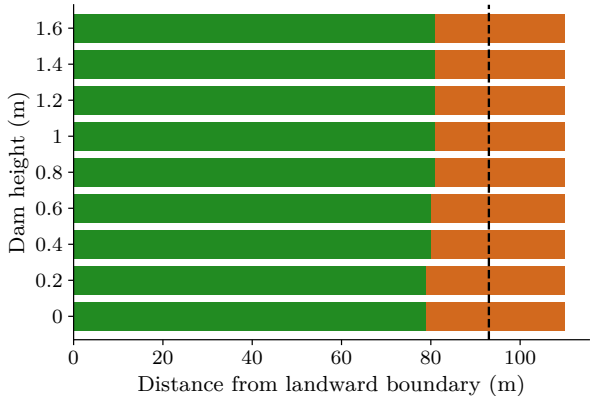

Figure 21: *Predicted vegetation establishment when the model domain contains dams of varying heights above the bed and is forced with increased water levels with 29.6 cm, as a result of 80 years of sea level rise. The black dotted line represents the location of the brushwood dam on the Marconi salt marsh. Green is vegetated, whereas brown is bare.*

difference regarding the sediment trapping capacity in the year 2060 (Appendix G). Furthermore, the dam height that results in the highest sedimentation rate landward of the dam shifts to higher values when the water level increases due to sea level rise (Appendix G).

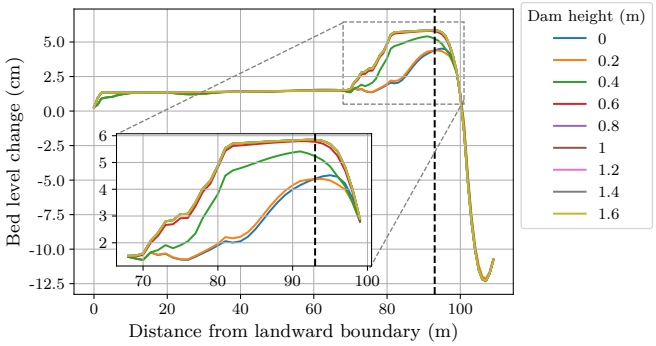

Figure 22: *Simulated bed level change values during one growing season in the year 2060 for a distance between 0 and 110 m of the landward boundary. Positive values mean that sedimentation has occurred, whereas negative values indicate erosion. The box shows the zoomed in changes landward and seaward of the dam, where the orange dotted line marks the sedimentation threshold for vegetation establishment (δz_{max}).*

3.3.2 Sea level rise scenario

To simulate the effects of predicted sea level rise the coming decades in the current salt marsh configuration of Marconi with a dam height of 0.4 m above the bed, the measured water level in 2021 was increased with 7.6 cm/decade. The vegetation boundary moves landward with approximately two meter per decade until the year 2060 (Figure 23). These relatively small shifts of the vegetation boundary can be exclusively explained by the increased water level resulting in a higher inundation percentage exceeding the threshold χ_{max}. From the year 2060 onward the vegetation boundary moves landward with larger steps per decade until eventually in the year 2100, only one meter of vegetation is left on the salt marsh.

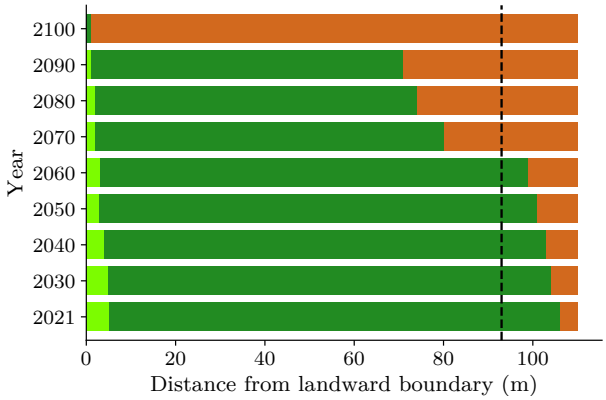

Figure 23: *Predicted vegetation establishment under the influence of sea level rise with increments of 7.6 cm/decade. The black line represents the location of the brushwood dam on the Marconi salt marsh. Dark green represents vegetated areas on a bathymetry after the construction of the Marconi salt marsh and light green on a bathymetry before the construction (Figure 12). Brown shows bare areas without vegetation.*

The vegetation boundary before the construction of the Marconi salt marsh stretches only to a maximum of five meter seaward of the landward boundary (Figure 23) in the year 2021. From 2040 onward the vegetation boundary gradually moves towards the landward boundary, until in 2100 no vegetation is left on the salt marsh.

4 Discussion

This study has extended the hydro-morphodynamic DET-ESTMORF model with vegetation dynamics based on morphodynamic and hydrodynamic thresholds extracted from field data. The model is therefore an efficient method to predict where pioneer vegetation will establish on salt marshes under certain environmental conditions or management measures.

4.1 Modelling salt marshes

The one-dimensional DET-ESTMORF model simulates changes in bed level caused by cross-shore flows and waves during each high tide. This makes it a really quick and efficient tool to evaluate morphodynamics and vegetation establishment patterns, however, it has some limitations. Alongshore components are not included in the model. Strong alongshore currents could lead to erosion on the lower elevated parts of a salt marsh, but it was previously shown that the high marsh dynamics are mainly ruled by cross-shore currents [59]. Furthermore, the underlying assumption was made that no sedimentation or erosion processes take place during low tide. Despite the fact that changes in bed level in the top layer of the salt marsh are predominantly caused by hydrodynamic forcing [28], aeolian transport and subsidence during low tide

might also induce morphodynamic changes [60]. This could be one reason that some erosion was measured in the field during growing season, especially in the plots closer to the sea (Figure 13), whereas the DET-ESTMORF model only simulated accretion under corresponding conditions (Figure 19). Another reason can be the presence of a migrating sand bank on the Marconi salt marsh that induces changes in the bed level that are not simulated by the model. To assess whether other processes than hydrodynamic forcing induce bed level change, the salt marsh bed should be continuously monitored, so that bed level change is also observed when the salt marsh is not inundated.

Additionally, the DET-ESTMORF model requires water level, significant wave height and peak wave period data as input. The latter two have been calculated with Bretschneider equations [52]. In order to check the validity of the resulting significant wave heights at this specific location, the values have been compared to previously modeled values by Van Maren., 2016 [61] in the same estuary. It appeared that both were in the same order of magnitude.

4.1.1 Section G

Measurements from the field have shown that a lot of erosion takes place at the seaward side of section G (Figure 13). The upper layer generally contains fine sand particles in the range of 63 to 150 μm [28]. When implementing these sediment characteristics and the initial bathymetry of section G in the DET-ESTMORF model, the results after one growing season almost exclusively show accretion (Appendix H). Hence, other factors must determine the morphodynamic processes in section G than the ones included in the DET-ESTMORF model. Besides potential soil compaction, the erosion in the field could have been caused by the low elevation (Figure 10) and by the heterogeneous nature of the soil, containing predominantly sand with chuncks of clay. Hence, cohesive forces are more or less absent in the soil of section G. Furthermore, the protective brushwood dam in section G is almost empty of wooden twigs caused by hydrodynamic forcing (Figure 24), so the attenuating function of the dam is limited. Above all, from the fact that the brushwood dam in section E is still in tact (Figure 24), it can be deduced that hydrodynamic forcing in section G is generally larger than in section E.

4.1.2 Protective structures

The desired effect of implementing a (brushwood) dam in Nature-based Solutions is to enhance sediment accretion in order to improve conditions for vegetation establishment [62, 19]. Aforementioned increase in sedimentation processes, compared to a case with no dam, was demonstrated for dams with an elevation equal to and larger than 0.4 m above the bed: the accretion landward of a dam significantly increases with dam heights ranging from 0.4 up to 1 m above the bed (Appendix G).

The brushwood dam present on the Marconi salt marsh was simulated in the DET-ESTMORF model by increasing the bed level elevation to the dam height before calculating the wave-induced bed shear stress. However, this approach has a limitation: it does simulate the height of the dam, but the permeability of the actual brushwood dam (Figure 24) in the field is not included herein. The drag coefficient of a semi-permeable dam (brushwood dam in the field) is lower than the drag coefficient of an impermeable dam (modelled dam) [63]. Therefore this approach may have resulted in an overestimation of the wave-induced bed shear stress attenuation capacity of the protective dam in the model, provoking higher sedimentation rates than the actual ones. Possible alternatives for a more process-based implementation of the semi-permeable brushwood are by activating wave damping through vegetation in SWAN or by using a two-dimensional model, where semipermeable boundaries can be implemented at cell edges. However, the latter method is inherent to higher computation time, that is why the current method was used.

Figure 24: *Above: Brushwood dam present in section G of the Marconi salt marsh. Compared to the dam in section E (below) this one is almost empty from horizontally oriented twigs. Below: Snapshot of brushwood dam located at section E of the Marconi salt marsh. It was constructed by implementing vertical wooden poles into the soil along two alongshore transects after which the gap between the transects was filled up with wooden twigs and secured with steel wire.*

4.1.3 Modelling vegetation dynamics

This study used monthly morpho- and hydrodynamic thresholds for the prediction of vegetation establishment. Alternatively, other methods for the prediction of vegetation establishment exist, such as the Window-of-Opportunity theory [64]. This method differs from monthly thresholds by the time-scale of the thresholds, but the underlying vegetation establishment-limiting processes are the same. However, a limitation of the monthly threshold method used is that short-term vegetation establishment-limiting processes, such as storms, were not taken into account. When values for short-term thresholds are known from the field, they can be added to improve the vegetation prediction capability of the model.

4.2 Monitoring salt marshes

Knowledge on environmental factors playing a role in the establishment of pioneer vegetation has expanded in recent years, because of the importance in the prediction of salt marsh development [65, 24]. However, there are still some missing pieces, specifically in the case of semi-natural salt marshes that have been designed under certain management criteria (e.g. structures or soil composition). So far it is known that seedlings need an inundation-free period to establish and that bed level change should not be too extreme to bury or uproot the young plant [24, 25, 26]. Nonetheless, the exact quantification of these limiting processes on a constructed salt marsh and the effects of protective structures remains absent [64]. Therefore this study focused on assessing the thresholds for hydrodynamic and morphodynamic processes limiting the vegetation establishment on a semi-natural salt marsh with implemented brushwood dam (*Marconi*). It was shown here that pioneer vegetation establishment can be explained by the monthly bed level change processes staying within 0.8 cm erosion and 1.4 cm sedimentation, while the inundation percentage should not increase 12%. These boundaries were determined based on the extreme cases of measured prevailing environmental factors in the field where vegetation was still present. However, vegetation was able to grow on areas a little further seaward in the field than measured. Hence, due to the absence of measurements in a higher range of prevailing processes, the actual value for the thresholds in fact might have been somewhat higher.

The found values of the morphodynamic thresholds were compared to a similar type of threshold determined with flume experiments with a different kind of salt marsh vegetation *Spartina* [66, 65]. The determined thresholds for vegetation establishment were the growth rate of the root (5 mm/week) and shoot (15 mm/week) of *Spartina*, because too much sedimentation buries the specimen, whereas too much erosion will cause it to slip out of the soil. These growth rates translate to erosion and sedimentation thresholds of roughly 2 and 6 cm/month respectively. Average growth rates for the shoot and root of *Salicornia* found in this study were in the same order of magnitude (Figure 16 and 17), whereas the morphodynamic thresholds for vegetation establishment have much smaller values (-0.8 and 1.4 cm/month, Figure 14). A possible explanation for this difference might be that vegetation units grew under controlled and idealised conditions in the previous study [66], whereas the thresholds in this study were based on vegetation growing in the field, where processes like competition and extreme weather conditions might hamper vegetation development and thereby affect how much stress they can withstand [67].

4.2.1 Bed level change

Measured bed level changes on the Marconi salt marsh were compared to morphodynamics of other salt marshes, in order to assess whether the study site behaves in a similar fashion. Willemsen, 2018 [26] found monthly bed level changes at the Dutch Westerschelde estuary to be between -100 and 100 mm. Elschot, 2020 [68] found annual net accretion values for several salt marshes along the Dutch northern coast to vary in a range between 7 and 22 mm, whereas Kennish, 2001 [69] found annual ranges between 1.3 and 18 mm for Atlantic and Gulf Coast marsh systems. The measured monthly bed level changes on the Marconi salt marsh ranges from -80 to 40 mm, falling within the range measured by Willemsen, 2018. When adding the average bed level changes over the months measured on Marconi landward of the brushwood dam (ignoring the migrating sand bank), it results in a net value of 10 mm accretion after one growing season. One must note that winter season is not taken into account here, where higher waves and higher occurrences of storms generally result in negative bed level change [70]. Hence, the annual bed level change behaviour on the Marconi salt marsh is in some measure comparable to other salt marshes [68, 69].

4.2.2 Vegetation dynamics

The measured root length of the vegetation growing under sandy conditions (section G) was consistently and significantly larger than those growing in more muddy conditions (section E) (Figure 16). This difference might be caused by the growth being adapted to the larger bed level change magnitudes (Figure 13) or due to lower availability of nutrients and moisture content in sandy compared to muddy soils [71]. The latter could also explain why, even though the bed level of section G is elevated in general approximately 20 cm higher than section E (Figure 10), vegetation was less abundant in section G than in section E (Table 1).

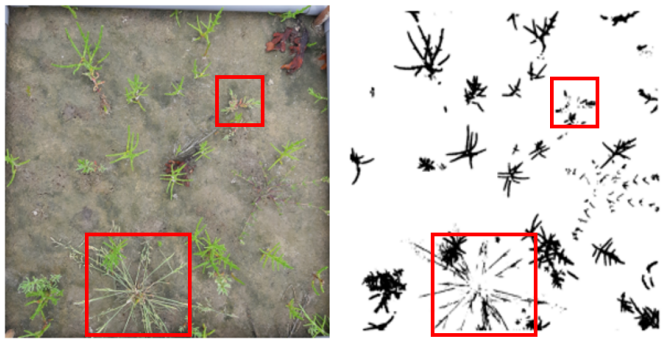

Figure 25: *Categorisation of pixels from a photograph taken from plot G8 the 30th of July (left) in background and vegetation (right). The red squares indicate other vegetation species than Salicornia on the actual photograph being included in the black pixels categorised as vegetation.*

The pixel classification method used to determine the FVC of each vegetation plot was not able to distinguish between different types of vegetation: it only categorised vegetation pixels (green) from background pixels (not green). Other vegetation growing on the Marconi salt marsh, e.g. *Suadea maritima*, was hence included in the number of vegetation pixels (Figure 25). Furthermore, in some cases salt was deposited on the *Salicornia* vegetation units, coloring them grey. Accordingly, these pixels were not included in the vegetation category. This caused some of the determined values for FVC to be exaggerated and others to be underestimated compared to the actual

vegetation cover of the plot. The only case in which the FVC was adjusted based on visual clues of the photograph was when the vegetation plot was covered in green algal mats. All in all, this pixel classification method is not able to distinguish between different types of vegetation, but provides a good indicator of the total fractional vegetation cover.

4.3 Implications for Nature-based Solutions

Implementations of NbS for the ever increasing importance of coastal protection in the face of climate change are globally expanding [16, 5, 72]. Hybrid engineering designs that combine vegetated foreshores with conventional structures not only enhance wave attenuation and increase stability and height of the foreshore, but also contribute to ecosystem values [15]. Previous research together with the current study can add to better designs for salt marsh establishment or restoration projects, since the developed model can be used to explore the effects of management measures, e.g. implementation of different types of structures or adjusting the (initial) elevation of the bed.

Something important to consider is that the boundaries implemented in this model and growth curves were based on a field study of a semi-natural salt marsh enclosed with brushwood dams and with the dominant pioneer species being *Salicornia*. The found relations and thresholds might not be one-to-one applicable to NbS with different environmental conditions and different pioneer vegetation. When evaluating other locations, the grid and boundary conditions change accordingly. Furthermore, thresholds for vegetation establishment can differ, dependent on the type of vegetation. For instance, *Spartina* is known to be less tolerant to high frequency salinity changes compared to *Salicornia* [73], hence the hydrodynamic threshold for vegetation establishment on a salt marsh with dominant pioneer vegetation being *Spartina* may be lower.

4.3.1 Protective structures

Simulations of one growing season have shown that increased height of a brushwood dam does not lead to much variation in the short-term location of the vegetation boundary. However, increasing the dam height does indeed lead to increased sedimentation effects landward of the dam. When taking into account that the increased accretion rate sustains through the subsequent years, it can be expected that the resulting higher bed levels will eventually contribute to less inundation of the salt marsh, and hence vegetation to establish on more seaward located areas.

Under the prevailing conditions in the year 2021 the optimal dam height was 0.4 m above the bed for the highest accretion rate landward of the dam. This is exactly the dam height that is implemented in the field at Marconi. However, due to a climate change-induced increased sea level, the optimal dam height shifted to higher values (Appendix G) moving ahead in time. This can be an indication that accretion on NbS can be stimulated by step-wise elevation of the dam height the coming decades or that NbS still in the planning phase should consider relatively high dam heights to insure optimal accretion landward of the dam the coming decades.

4.3.2 Sea level rise

Climate change-driven sea level rise has a large impact on the viability of the restoration or establishment of Nature-based Solutions. Relative sea level rise is site-specific, depending on other factors than global sea level rise alone, such as changing ocean currents and local land uplift or subsidence [74]. Therefore, generalisation of the local effects of global sea level rise is not useful [11]. The extended DET-ESTMORF model, as long as its calibrated on the right location, could provide a tool in demonstrating the local effects of sea level rise on the establishment of pioneer vegetation on a (semi-natural) salt marsh. This study simulated the local effects of a sea level rise rate resulting from the intermediate greenhouse gas emission scenario [56] on the vegetation boundary on the Marconi salt marsh. Results show that the vegetation boundary moves toward the coast with small steps at first, but eventually rapid retreat of the boundary takes place until vegetation has more or less disappeared in the year 2100 (Figure 23). However, it must be remarked that for computation efficiency the sea level rise scenario has been applied with increments of decades, so the bathymetry did not have a change to evolve for the nine subsequent years every increment. The capability of salt marshes to respond morphodynamically to sea level rise by vertical accretion and/or lateral expansion [75] has been downplayed in this scenario, so the simulated landward movement of the vegetation boundary the coming century might have been exaggerated.

When simulations show that the vegetation boundary is retreating on the long term as a result of increased inundation, appropriate management measures can be taken in the design process to combat these effects, such as thin-layer sediment placement to counter the increased inundation percentage without exceeding the sedimentation threshold [76]. Applying the sea level rise scenario on the bathymetry of Marconi before the construction works has proven that increasing the overall elevation does actually have a major beneficial effect on vegetation establishment on the Nature-based Solution (Figure 23). The model can hence be used to assess what the most optimal bed level elevation would be under different sea level rise scenarios.

4.3.3 Quantification of ecosystem services

Although it is known what type of ecosystem services salt marshes provide, their quantification is somewhat falling behind [77, 78]. This model could be used as a tool for the quantification of coastal protection, but some additional steps are required. Wave attenuation and sediment trapping by salt marsh vegetation play a large role in the coastal protection function [10, 79]. Currently, the extended DET-ESTMORF model simulates interactions in only one direction: the effect of morphodynamic and hydrodynamic processes on the vegetation establishment. However, to make a translation towards quantification of the wave attenuating function of the growing pioneer vegetation, the number of vegetation units making up for a cer-

tain fractional vegetation cover should be determined in order to specify the actual number of vegetation units present. This number combined with the average frontal area of a vegetation unit provides an estimate of the wave attenuation rendered by the total vegetation coverage of the salt marsh. Furthermore, salt marsh vegetation generally experiences a positive feedback between growth and sediment deposition [80]. These two aforementioned feedback-mechanisms should in turn be implemented in the model to increase the accuracy of vegetation establishment predictions and of the ecosystem service quantification.

5 Conclusion

The hydro-morphodynamic model was extended to simulate pioneer vegetation establishment under various conditions and could therefore be used to answer the main question of this paper *'What are the effects of protective structures and climate change-driven sea level rise on the establishment of pioneer vegetation on Nature-based Solutions?'*.

Implementing structures on NbS does not lead to a large difference in the location of the vegetation boundary, but it does lead to increased sedimentation rates behind the structure. Furthermore, the optimal height of the implemented structure with respect to the highest sedimentation rate shifted to higher values when the water level increased due to sea level rise.

Predicted sea level rise causes the vegetation boundary to retreat towards the coast with small steps the first couple of decades, because the hydrodynamic threshold is exceeded on more locations due to the increased water level. However, from the year 2070 the vegetation boundary moved towards the coast with significantly larger steps per decade, until in the year 2100 only 1 m of vegetation is present on the simulated nature-based solution. Simulations show that increasing the bed level elevation can stimulate vegetation growth on a NbS.

All in all, this study has shown that the extended DETESTMORF model can accurately predict the pioneer vegetation boundary on Nature-based Solutions under different environmental circumstances and with different implemented management measures. Besides the location of vegetation establishment, the growth of the root and shoot of the pioneer species *Salicornia* can be estimated with the found growth relations.

References

[1] E. Barbier, S. D. Hacker, C. Kennedy, E. W. Koch, A. C. Stier, and B. R. Silliman, "The value of estuarine and coastal ecosystem services," *Ecological Monographs*, vol. 81, no. 2, pp. 169–193, 2011.

[2] D. F. Boesch and R. E. Turner, "Dependence of fishery species on salt marshes: The role of food and refuge," *Estuaries*, vol. 7, no. 4, pp. 460–468, 1984.

[3] M. R. Van Eerden, R. H. Drent, J. Stahl, and J. P. Bakker, "Connecting seas: Western Palaearctic continental flyway for water birds in the perspective of changing land use and climate," *Global Change Biology*, vol. 11, no. 6, pp. 894–908, 2005.

[4] C. M. Duarte, I. J. Losada, I. E. Hendriks, I. Mazarrasa, and N. Marbà, "The role of coastal plant communities for climate change mitigation and adaptation," *Nature Climate Change*, vol. 3, no. 11, pp. 961–968, 2013.

[5] S. Temmerman, P. Meire, T. J. Bouma, P. M. J. Herman, T. Ysebaert, and H. J. De Vriend, "Ecosystem-based coastal defence in the face of global change," *Nature*, vol. 504, no. 7478, pp. 79–83, 2013.

[6] S. Narayan, M. W. Beck, B. G. Reguero, I. J. Losada, B. Van Wesenbeeck, N. Pontee, J. N. Sanchirico, J. C. Ingram, G. M. Lange, and K. A. Burks-Copes, "The effectiveness, costs and coastal protection benefits of natural and nature-based defences," *PLoS ONE*, vol. 11, no. 5, pp. 1–17, 2016.

[7] M. D. Spalding, S. Ruffo, C. Lacambra, I. Meliane, L. Z. Hale, C. C. Shepard, and M. W. Beck, "The role of ecosystems in coastal protection: Adapting to climate change and coastal hazards," *Ocean and Coastal Management*, vol. 90, pp. 50–57, 2014.

[8] K. S. Dijkema, *Changes in salt-marsh area in the Netherlands Wadden Sea after 1600*, pp. 42–51. Dordrecht: Springer Netherlands, 1987.

[9] P. Adam, "Saltmarshes in a time of change," *Environmental Conservation*, vol. 29, pp. 39–61, 2002.

[10] C. C. Shepard, C. M. Crain, and M. W. Beck, "The Protective Role of Coastal Marshes: A Systematic Review and Meta-analysis," *PLOS ONE*, vol. 6, no. 11, pp. 1–11, 2011.

[11] P. Adam, "Chapter 23 - Salt Marsh Restoration," in *Coastal Wetlands* (G. M. E. Perillo, E. Wolanski, D. R. Cahoon, and C. S. Hopkinson, eds.), pp. 817–861, Elsevier, 2019.

[12] S. Best, M. Van der Wegen, J. Dijkstra, P. W. Willemsen, B. W. Borsje, and D. J. Roelvink, "Do salt marshes survive sea level rise? Modelling wave action, morphodynamics and vegetation dynamics," *Environmental Modelling and Software*, vol. 109, no. August, pp. 152–166, 2018.

[13] K. B. Gedan, M. L. Kirwan, E. Wolanski, E. B. Barbier, and B. R. Silliman, "The present and future role of coastal wetland vegetation in protecting shorelines: Answering recent challenges to the paradigm," *Climatic Change*, vol. 106, no. 1, pp. 7–29, 2011.

[14] D. R. Cahoon, K. L. McKee, and James Morris, "How plants influence resilience of salt marsh and mangrove wetlands to sea-level rise," *Estuaries and Coasts*, vol. 44, pp. 883–898, 2021.

[15] B. W. Borsje, B. K. van Wesenbeeck, F. Dekker, P. Paalvast, T. J. Bouma, M. M. van Katwijk, and M. B. de Vries, "How ecological engineering can serve in coastal protection," *Ecological Engineering*, vol. 37, no. 2, pp. 113–122, 2011.

[16] M. Wolters, A. Garbutt, and J. P. Bakker, "Salt-marsh restoration: Evaluating the success of de-embankments in north-west Europe," *Biological Conservation*, vol. 123, no. 2, pp. 249–268, 2005.

[17] R. S. Warren, P. E. Fell, R. Rozsa, A. H. Brawley, A. C. Orsted, E. T. Olson, V. Swamy, and W. A. Niering, " SEPTEMBER 2002 Restoration Ecology Vol. 10 No. 3, pp. 497–513 497 © 2002 Society for Ecological Restoration Salt Marsh Restoration in Connecticut- 20 Years of Science and Management," vol. 10, no. 3, pp. 497–513, 2002.

[18] J. P. Bakker, P. Esselink, K. S. Dijkema, W. E. van Duin, and D. J. de Jong, "Restoration of salt marshes in the Netherlands," *Hydrobiologia*, vol. 478, no. 1, pp. 29–51, 2002.

[19] J. C. Winterwerp, T. Albers, E. J. Anthony, D. A. Friess, A. G. Mancheño, K. Moseley, A. Muhari, S. Naipal, J. Noordermeer, A. Oost, C. Saengsupavanich, S. A. Tas, F. H. Tonneijck, T. Wilms, C. Van Bijsterveldt, P. Van Eijk, E. Van Lavieren, and B. K. Van Wesenbeeck, "Managing erosion of mangrove-mud coasts with permeable dams – lessons learned," *Ecological Engineering*, vol. 158, no. November, p. 106078, 2020.

[20] P. W. Willemsen, *Biogeomorphology of salt marshes*. PhD thesis, University of Twente, 2021.

[21] T. J. Bouma, J. van Belzen, T. Balke, J. van Dalen, P. Klaassen, A. M. Hartog, D. P. Callaghan, Z. Hu, M. J. Stive, S. Temmerman, and P. M. Herman, "Short-term mudflat dynamics drive long-term cyclic salt marsh dynamics," *Limnology and Oceanography*, vol. 61, no. 6, pp. 2261–2275, 2016.

[22] S. Silvestri and M. Marani, "Salt-Marsh Vegetation and Morphology: Basic Physiology, Modelling and Remote Sensing Observations," *The Ecogeomorphology of Tidal Marshes*, no. March, pp. 5–25, 2004.

[23] I. Townend, C. Fletcher, M. Knappen, and K. Rossington, "A review of salt marsh dynamics," *Water and Environment Journal*, vol. 25, no. 4, pp. 477–488, 2011.

[24] T. Balke, P. M. Herman, and T. J. Bouma, "Critical transitions in disturbance-driven ecosystems: Identifying windows of opportunity for recovery," *Journal of Ecology*, vol. 102, no. 3, pp. 700–708, 2014.

[25] Z. Hu, J. Van Belzen, D. Van Der Wal, T. Balke, Z. B. Wang, M. Stive, and T. J. Bouma, "Windows of opportunity for salt marsh vegetation establishment on bare tidal flats: The importance of temporal and spatial variability in hydrodynamic forcing," *Journal of Geophysical Research G: Biogeosciences*, vol. 120, no. 7, pp. 1450–1469, 2015.

[26] P. W. Willemsen, B. W. Borsje, S. J. Hulscher, D. Van der Wal, Z. Zhu, B. Oteman, B. Evans, I. Möller, and T. J. Bouma, "Quantifying Bed Level Change at the Transition of Tidal Flat and Salt Marsh: Can We Understand the Lateral Location of the Marsh Edge?," *Journal of Geophysical Research: Earth Surface*, vol. 123, no. 10, pp. 2509–2524, 2018.

[27] E.-J. Houwing, "Morphodynamic development of intertidal mudflats: consequences for the extension of the pioneer zone," *Continental Shelf Research*, vol. 20, no. 12, pp. 1735–1748, 2000.

[28] B. de Vries, P. Willemsen, M. E. B. van Puijenbroek, L. Coumou, M. Baptist, J. Clveringa, P. Dankers, and K. Elschot, "Salt marsh pilot Marconi- Monitoring results," tech. rep., 2021.

[29] D. Dillingh, *Kenmerkende waarden kustwateren en grote rivieren*. 2013.

[30] P. Sadeghi-Tehran, N. Virlet, K. Sabermanesh, and M. J. Hawkesford, "Multi-feature machine learning model for automatic segmentation of green fractional vegetation cover for high-throughput field phenotyping," *Plant Methods*, vol. 13, no. 1, pp. 1–16, 2017.

[31] G. E. Meyer and J. C. Neto, "Verification of color vegetation indices for automated crop imaging applications," *Computers and Electronics in Agriculture*, vol. 63, no. 2, pp. 282–293, 2008.

[32] M. van Regteren, I. Colosimo, P. de Vries, M. E. B. van Puijenbroek, V. S. Freij, M. J. Baptist, and K. Elschot, "Limited seed retention during winter inhibits vegetation establishment in spring, affecting lateral marsh expansion capacity," *Ecology and Evolution*, vol. 9, no. 23, pp. 13294–13308, 2019.

[33] Arcadis, "Hydromorfologie Eems-Dollard Estuarium," Tech. Rep. december, 2013.

[34] J. A. Nelder, "The Fitting of a Generalization of the Logistic Curve," *Biometrics*, vol. 17, pp. 89–110, dec 1961.

[35] Z. B. Wang, H. J. De Vriend, M. J. Stive, and I. H. Townend, "On the parameter setting of semi-empirical long-term morphological models for estuaries and tidal lagoons," *River, Coastal and Estuarine Morphodynamics: RCEM 2007 - Proceedings of the 5th IAHR Symposium on River, Coastal and Estuarine Morphodynamics*, vol. 1, pp. 103–111, 2008.

[36] Z. Hu, Z. B. Wang, T. J. Zitman, M. J. Stive, and T. J. Bouma, "Predicting long-term and short-term tidal

flat morphodynamics using a dynamic equilibrium theory," *Journal of Geophysical Research F: Earth Surface*, vol. 120, no. 9, pp. 1803–1823, 2015.

[37] Z. B. Wang and I. H. Townend, "Influence of the nodal tide on the morphological response of estuaries," *Marine Geology*, vol. 291-294, pp. 73–82, 2012.

[38] Z. Wang, B. Karssen, R. Fokkink, and A. Langerak, "A dynamic-empirical model for estuarine morphology," *Physics of Estuaries and Coastal Seas: Proceedings of the 8th International Biennial Conference on Physics of Estuaries an Coastal Seas*, 1998.

[39] J. C. Winterwerp and W. van Kesteren, *Introduction to the physics of cohesive sediment in the marine environment*. Elsevier, developmen ed., 2004.

[40] L. O. Amoudry and A. J. Souza, "Deterministic coastal morpohological and sediment transport modeling: a review and discussion," *Reviews of Geophysics*, vol. 49, no. 2, 2011.

[41] Z. B. Wang, H. de Vriend, M. Stive, and I. Townend, "On the parameter setting of semi-empirical long-term morphological models for estuaries and tidal lagoons," *River, Coastal and Estuarine Morphodynamics*, pp. 103–111, sep 2007.

[42] L. C. van Rijn, "Unified View of Sediment Transport by Currents and Waves. III: Graded Beds," *Journal of Hydraulic Engineering*, vol. 133, no. 7, pp. 761–775, 2007.

[43] W. Roberts, P. Le Hir, and R. J. S. Whitehouse, "Investigation using simple mathematical models of the effect of tidal currents and waves on the profile shape of intertidal mudflats," *Continental Shelf Research*, vol. 20, no. 10, pp. 1079–1097, 2000.

[44] X. J. Liu, S. Gao, and Y. P. Wang, "Modeling profile shape evolution for accreting tidal flats composed of mud and sand: A case study of the central Jiangsu coast, China," *Continental Shelf Research*, vol. 31, no. 16, pp. 1750–1760, 2011.

[45] C. T. Friedrichs and D. G. Aubrey, "Uniform Bottom Shear Stress and Equilibrium Hyposometry of Intertidal Flats," in *Mixing in Estuaries and Coastal Seas*, ch. 24, pp. 405–429, American Geophysical Union (AGU), 1996.

[46] P. L. Hir, W. Roberts, O. Cazaillet, M. Christie, P. Bassoullet, and C. Bacher, "Characterization of intertidal flat hydrodynamics," *Continental Shelf Research*, vol. 20, pp. 1433–1459, 2000.

[47] A. D'Alpaos, S. Lanzoni, S. M. Mudd, and S. Fagherazzi, "Modeling the influence of hydroperiod and vegetation on the cross-sectional formation of tidal channels," *Estuarine, Coastal and Shelf Science*, vol. 69, no. 3, pp. 311–324, 2006.

[48] N. Booij, R. C. Ris, and L. H. Holthuijsen, "A third-generation wave model for coastal regions 1. Model description and validation," *Journal of Geophysical Research: Oceans*, vol. 104, no. C4, pp. 7649–7666, 1999.

[49] K. Hasselmann, T. Barnett, E. Bouws, H. Carlson, D. Cartwright, K. Enke, J. Ewing, H. Gienapp, D. Hasselmann, P. Kruseman, A. Meerburg, P. Muller, D. Olbers, K. Richter, W. Sell, and H. Walden, "Measurements of wind-wave growth and swell decay during the Joint North Sea Wave Project (JONSWAP)," *Deut. Hydrogr. Z.*, vol. 8, pp. 1–95, 1973.

[50] R. Soulsby, *Bed shear-stresses due to combined waves and currents*. Delft Hydraulics, 1995.

[51] D. S. Van Maren, A. P. Oost, Z. B. Wang, and P. C. Vos, "The effect of land reclamations and sediment extraction on the suspended sediment concentration in the Ems Estuary," *Marine Geology*, vol. 376, pp. 147–157, 2016.

[52] C. L. Bretschneider, "Generation of waves by wind: State of the art," 1964.

[53] A. Calderon, A. Smale, J. Nieuwkoop, and J. Morris, "Input database for the Bretschneider wave calculations for narrow river areas," 2016.

[54] J. P. de Waal, "Windmodellering voor bepaling waterstanden en golven," *Een analyse van de bouwstenen. Werkdocument Rijkswaterstaat/RIZA*, 2003.

[55] L. Rijn, "Principles of sediment transport in rivers, estuaries and coastal seas," 1993.

[56] IPCC, "Climate Change 2021: The Pysical Science Basis.," tech. rep., Cambrigde University Press, 2021.

[57] D. J. Reed, "The response of coastal marshes to sea-level rise: Survival or submergence?," *Earth Surface Processes and Landforms*, vol. 20, pp. 39–48, feb 1995.

[58] C. Craft, J. Clough, J. Ehman, S. Joye, R. Park, S. Pennings, H. Guo, and M. Machmuller, "Forecasting the effects of accelerated sea-level rise on tidal marsh ecosystem services," *Frontiers in Ecology and the Environment*, vol. 7, no. 2, pp. 73–78, 2009.

[59] Y. Wang, Y. P. Wang, Q. Yu, Z. Du, Z. B. Wang, and S. Gao, "Sand-Mud Tidal Flat Morphodynamics Influenced by Alongshore Tidal Currents," *Journal of Geophysical Research: Oceans*, vol. 124, no. 6, pp. 3818–3836, 2019.

[60] Z. Hu, W. Lenting, D. van der Wal, and T. J. Bouma, "Continuous monitoring bed-level dynamics on an intertidal flat: Introducing novel, stand-alone high-resolution SED-sensors," *Geomorphology*, vol. 245, pp. 223–230, 2015.

[61] B. Van Maren, J. Vroom, T. Vijverber, M. Schoemans, and A. Van Rooijen, "Mud dynamics in the Ems-Dollard, phase 2," 2014.

[62] V. Vuik, B. W. Borsje, P. W. Willemsen, and S. N. Jonkman, "Salt marshes for flood risk reduction: Quantifying long-term effectiveness and life-cycle costs," *Ocean and Coastal Management*, vol. 171, pp. 96–110, 2019.

[63] A. Gijón Mancheño, W. Jansen, W. S. Uijttewaal, A. J. Reniers, A. A. van Rooijen, T. Suzuki, V. Etminan, and J. C. Winterwerp, "Wave transmission and drag coefficients through dense cylinder arrays: Implications for designing structures for mangrove restoration," *Ecological Engineering*, vol. 165, no. October 2020, 2021.

[64] T. Balke, T. J. Bouma, E. M. Horstman, E. L. Webb, P. L. Erftemeijer, and P. M. Herman, "Windows of opportunity: Thresholds to mangrove seedling establishment on tidal flats," *Marine Ecology Progress Series*, vol. 440, no. October, pp. 1–9, 2011.

[65] D. W. Poppema, P. W. Willemsen, M. B. de Vries, Z. Zhu, B. W. Borsje, and S. J. Hulscher, "Experiment-supported modelling of salt marsh establishment," *Ocean and Coastal Management*, vol. 168, no. November 2018, pp. 238–250, 2019.

[66] H. Cao, Z. Zhu, T. Balke, L. Zhang, and T. J. Bouma, "Effects of sediment disturbance regimes on Spartina seedling establishment: Implications for salt marsh creation and restoration," *Limnology and Oceanography*, vol. 63, no. 2, pp. 647–659, 2018.

[67] H. Poorter, F. Fiorani, R. Pieruschka, T. Wojciechowski, W. H. van der Putten, M. Kleyer, U. Schurr, and J. Postma, "Pampered inside, pestered outside? Differences and similarities between plants growing in controlled conditions and in the field," *New Phytologist*, vol. 212, no. 4, pp. 838–855, 2016.

[68] K. Elschot, M. E. B. van Puijenbroek, D. Lagendijk, J. T. Wal, and C. Sonneveld, "Lange-termijnontwikkeling van kwelders in de Waddenzee (1960-2018)," 2020.

[69] M. J. Kennish, "Coastal Salt Marsh Systems in the U.S.: A Review of Anthropogenic Impacts," *Journal of Coastal Research*, vol. 17, pp. 731–748, dec 2001.

[70] T. J. Andersen, M. Pejrup, and A. A. Nielsen, "Long-term and high-resolution measurements of bed level changes in a temperate, microtidal coastal lagoon," *Marine Geology*, vol. 226, no. 1, pp. 115–125, 2006.

[71] H. N. Morzaria-Luna and J. B. Zedler, "Does seed availability limit plant establishment during salt marsh restoration?," *Estuaries and Coasts*, vol. 30, no. 1, pp. 12–25, 2007.

[72] L. Yuan, Y. H. Chen, H. Wang, H. B. Cao, Z. Y. Zhao, C. D. Tang, and L. Q. Zhang, "Windows of opportunity for salt marsh establishment: the importance for salt marsh restoration in the Yangtze Estuary," *Ecosphere*, vol. 11, no. 7, 2020.

[73] B. E. Mahall and R. B. Park, "The Ecotone Between Spartina Foliosa Trin. and Salicornia Virginica L. in Salt Marshes of Northern San Francisco Bay: II. Soil Water and Salinity," *Journal of Ecology*, vol. 64, pp. 793–809, oct 1976.

[74] S. Rahmstorf, "Sea-level rise: Towards understanding local vulnerability," *Environmental Research Letters*, vol. 7, no. 2, pp. 8–11, 2012.

[75] S. Fagherazzi, G. Mariotti, N. Leonardi, A. Canestrelli, W. Nardin, and W. S. Kearney, "Salt Marsh Dynamics in a Period of Accelerated Sea Level Rise," *Journal of Geophysical Research: Earth Surface*, vol. 125, no. 8, pp. 1–31, 2020.

[76] K. Raposa, K. Wasson, J. Nelson, M. Fountain, J. West, C. Endris, and A. Woolfolk, "Guidance for thin-layer sediment placement as a strategy to enhance tidal marsh resilience to sea level rise," tech. rep., 2020.

[77] C. P. Brisson, T. C. Coverdale, and M. D. Bertness, "Salt marsh die-off and recovery reveal disparity between the recovery of ecosystem structure and service provision," *Biological Conservation*, vol. 179, pp. 1–5, 2014.

[78] E. Barbier, "Valuing Ecosystem Services for Coastal Wetland Protection and Restoration: Progress and Challenges," *Resources*, vol. 2, no. 3, pp. 213–230, 2013.

[79] I. Möller, "Wave attenuation over coastal salt marshes under storm surge conditions — The Trilateral Cooperation on the Protection of the Wadden Sea," pp. 1–20, 2014.

[80] D. S. Srivastava and R. L. Jefferies, "The Effect of Salinity on the Leaf and Shoot Demography of Two Arctic Forage Species," *Journal of Ecology*, vol. 83, pp. 421–430, nov 1995.

A Measurements of vegetation characteristics

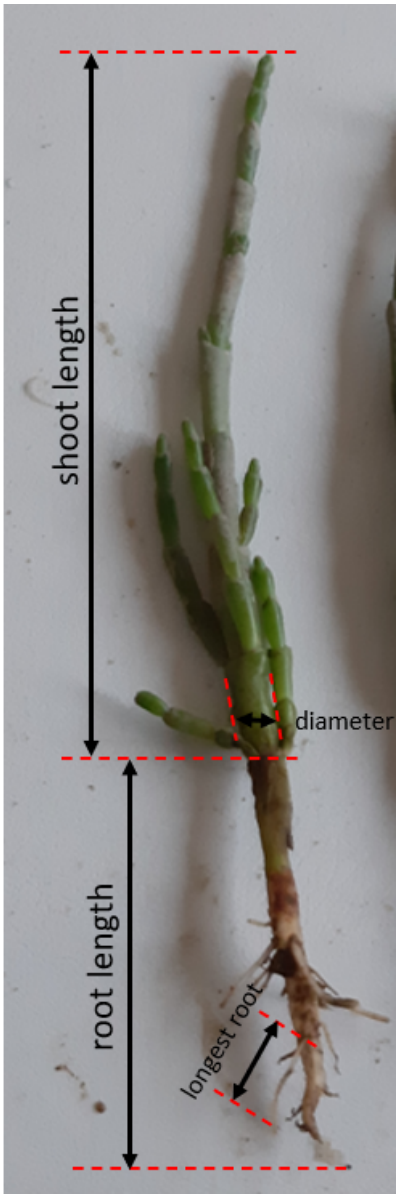

Measurement of vegetation characteristics shoot length, root length, longest root length, and diameter of the largest part of the shoot of Salicornia unit.

B DET-ESTMORF model parameters, description, used value and sources.

Model parameters that are used for the simulations with the DET-ESTMORF model, their description and units, their applied value and the source from which the applied value was obtained.

Parameter	Description	Value	Source
ρ_s	Density of sediment density (kg/m^3)	2650	Van Rijn, 2007 [42]
ρ_w	Density of water (kg/m^3)	1024	-
m_e	Erosion coefficient (kg/(m^2 · s))	0.00005	Roberts et al., 2000 [43]
f_c	Friction factor for currents (-)	0.002	Roberts et al., 2000 [43]
f_w	Friction factor for waves (-)	Equation 10	-
ν	Kinematic viscosity (m^2/s)	0.000001	-
D	Tide averaged diffusion coefficient (m^2/s)	30	Wang et al., 2008 [35]
n	Power for Equation 4	2	Wang et al., 2008 [35]
θ_α	Angle between currents and waves (°)	0	-
C_E	Constant overall sediment concentration (kg/m^3)	0.05	Van Maren, 2016 [51]
c_e	Local equilibrium sediment concentration (kg/m^3)	Equation 4	Wang et al., 2007 [41]
c	Sediment concentration (kg/m^3)	-	-
τ_{cr}	Critical shear stress for erosion (kg/(m · s^2))	Equation 22	Roberts et al., 2000 [43]
τ_E	Uniform equilibrium bed shear stress (kg/(m · s^2))	Equation 3	Winterwerp et al., 2004 [39]
τ_{90}	90th percentile bed shear stress in tidal cycle (kg/(m · s^2))	-	SWAN
τ_{cur}	Current-induced bed shear stress (kg/(m · s^2))	Equation 8	-
τ_{wave}	Wave-induced bed shear stress (kg/(m · s^2))	Equation 9	Soulsby, 1995 [50]
τ_m	Mean bed shear stress (kg/(m · s^2))	Equation 11	Soulsby, 1995 [50]
τ_{max}	Maximum bed shear stress (kg/(m · s^2))	Equation 12	Soulsby, 1995 [50]
w_s	Settling velocity for suspended sediment (m/s)	Equation 21	
h	water depth during high water (m)	-	-
t	Time (s)	-	-
x	Cross-shore coordinate (m)	-	-
p	Bed porosity (-)	0.6	Liu et al., 2011 [44]
z	Bed level (m+NAP)	-	-
ΔV	Volume of water (m^3)	-	-
u_c	Cross-shore current (m/s)	Equation 7	Hu et al., 2015 [36]
u_{wave}	Root-mean square of maximum orbital motion near bed (m/s)	-	SWAN
B	Unit alongshore width of flat	-	-
k_s	Nikuradse roughness length (m)	2.5 · D_{50}	-
ξ	Particle excursion amplitude close to bed (m)	-	SWAN
D_{50}	Mean sediment diameter (m)	-	De Vries et al., 2021 [28]
$D*$	Dimensionless sediment characteristic	Equation 23	Van Rijn, 1993 [55]
θ	Shields parameter	Equation 24	Van Rijn, 1993 [55]
s	Ratio between sediment and water	2.65	De Vries et al., 2021 [28]

C Fetch lengths

Division of the wind-wave-generating domain of the Marconi salt marsh in bins of 10 °for the calculation of fetch lengths with the Bretschneider equations.

D Erosion pin lengths

Lengths of erosion pins (cm) measured in the field during each field trip. The pin number 1 represents the erosion pin closest to the sea, whereas number 2 represents the one in the diagonal corner. In case no value is noted at a vegetation plot on a certain date, the erosion pins have disappeared from the field. In plot 2 from section G two erosion pins were implemented and measured in the field the 23th of April, but the field trip after, both of these erosion pins were gone. Therefore four new ones were placed back at this location.

Section	Plot	Pin	Date				
			23-04	02-06	01-07	30-07	28-09
E	**1**	**1**	101.2	101.1	101.9	-	-
		2	104.7	104.8	104.4	-	-
	2	**1**	100.5	100.6	99.6	100.2	101.4
		2	100.6	99.3	99.9	100	99.4
	3	**1**	101.8	101.4	101.3	101	100.9
		2	100.6	99.9	100.1	100	99
	4	**1**	103.5	103.1	101.5	101.4	101
		2	90.7	99.9	100.2	100	99.4
	5	**1**	90.2	92.1	90.3	90.7	91.2
		2	98.4	98.1	98.2	97.8	97.9
	6	**1**	99.4	99	99.4	98.8	97.2
		2	95.3	95.1	95.1	94.4	93.5
	7	**1**	99.2	98.9	98.8	98.5	98.3
		2	96.1	95.9	96.1	95.8	95.5
	8	**1**	96	95.8	95.6	95.5	95.5
		2	89.5	89.5	89.5	90	89.1
	9	**1**	90.6	90.5	90.7	90.3	90.2
		2	96.1	95.9	95.8	96	95.5
	10	**1**	100.3	100.4	100	99.2	100.3
		2	99	99.2	99.1	99.9	99.1
	11	**1**	91.4	91.5	91.2	91.1	91.2
		2	91.9	91.5	91.3	91.4	91.1
	12	**1**	93.6	93.3	93	93.4	93.2
		2	88.2	88.1	88.2	87.8	87.9
G	**1**	**1**	100	103.2	105	106	-
		2	100.5	102.1	104.3	102.1	-
	2	**1**	-	57.3	61.4	61.6	62.1
		2	-	48	52.1	51.4	52.8
		3	-	44.5	48.9	48.5	51.7
		4	-	40.3	40.2	44.3	43.8
	3	**1**	106.5	108.9	112.2	113.7	63.5
		2	104.8	110	112.9	-	-
	4	**1**	115.1	123.1	118.7	117.9	115.5
		2	115.5	122.5	121.2	118.9	116.7
	5	**1**	111.5	117.4	119	114.5	111.4
		2	111.2	116.3	119	115.1	114.9
	6	**1**	103.8	104.7	103.5	102	105.3
		2	103.6	104.2	102.7	103.1	103.4
	7	**1**	99.2	97.8	97	97	96.4
		2	100.2	98.7	97.4	97.3	97.5
	8	**1**	100.6	100	99	98.9	98.7
		2	101	100.5	100.2	100.1	100.2
	9	**1**	100.5	100.2	99.9	99.1	98.5
		2	100.6	100.6	100.4	99.7	100.1
	10	**1**	98.5	97.6	97.6	97.7	97.8
		2	98.4	97.6	97.7	97.1	97.3
	11	**1**	97.6	96.8	96.6	96.6	96.8
		2	98.6	98.2	98.5	98.2	97.8
	12	**1**	98.6	97.9	97.9	97.7	97.5
		2	97.6	97.1	97.3	96.9	96.5

E Vegetation data

Measured values of the vegetation characteristics shoot length, root length, longest root length, diameter of biggest part of the shoot, weight of the whole unit, and weight of the shoot during each field trip in sections E and G.

Section	Date	Plot	Shoot (cm)	Root (cm)	Longest root (cm)	Diameter (cm)	Weight (g)	Weight shoot (g)
G	**02-06**	**7**	2.4	2.1	1.5	0.34	0.14	0.1
			3.5	2.4	1.2	0.51	0.26	0.22
			1.2	1.2	0.6	0.45	0.14	0.11
			2.7	2.1	1.8	0.36	0.14	0.12
			2.7	3.1	1.6	0.45	0.22	0.2
		8	3	2.6	1	0.5	0.26	0.22
			2.3	2	1.8	0.35	0.12	0.1
			2	1.9	0.7	0.5	0.13	0.13
			2.5	1.9	1.1	0.5	0.16	0.15
			1.1	2	0.3	0.37	0.06	0.06
		9	1.5	1.8	0.9	0.41	0.08	0.06
			2.4	3.2	0.8	0.4	0.15	0.11
			1.6	1.9	1.7	0.34	0.07	0.07
			2	2.4	0	0.454	0.12	0.12
			1.1	1.5	1.6	0.34		
		10	2.1	2.1	2.2	0.53	0.15	0.14
			1.6	2.1	0.5	0.4	0.07	0.07
			2	1.5	0	0.46	0.14	0.13
			0.7	1.3	0	0.31		
			0.5	2	1.2	0.27		
		11	1.9	1.3	1.5	0.5	0.13	0.11
			0.7	1.5	0	0.33		
			0.4	1	0.5	0.25		
			2	2.5	0	0.48	0.14	0.14
		12	1.5	2	0.8	0.37	0.08	0.08
			2.4	2.5	2.3	0.48	0.21	0.18
			2	2.1	1.4	0.42	0.15	0.11
			2.1	1.8	1	0.47	0.14	0.09
			0.5	1.5	0.3	0.27		

Section	Date	Plot	Shoot (cm)	Root (cm)	Longest root (cm)	Diameter (cm)	Weight (g)	Weight shoot (g)
E	**02-06**	**2**	3	2	1.2	0.46	0.29	0.22
			2.5	1.8	2.6	0.44	0.2	0.17
			2	2.5	2	0.43	0.18	0.15
			1.3	2.1	0.4	0.36	0.11	0.08
			1.2	2.2	0	0.44	0.14	0.13
		3	2.9	2	1	0.42	0.24	0.19
			1.2	2.2	2	0.32	0.07	0.05
			2.8	2.9	2	0.48	0.26	0.21
			2.7	1.8	0.6	0.51	0.2	0.17
			-	-	-	-	-	-
		4	1.7	3	0.6	0.37	0.12	0.09
			1	2	0.4	0.26	0.07	0.04
			1.5	2.5	0.7	0.31	0.08	0.07
			0.5	2.5	0.9	0.26		<0.01
			0.5	2	0.9	0.26		<0.01
		5	1.7	2.5	1.8	0.29	0.1	0.06
			0.5	2	1	0.24	0.09	0.04
			0.7	1.6	1	0.28		<0.01
			1.7	2.5	1.2	0.34	0.11	0.09
			0.8	3	1.5	0.28		<0.04
		6	2	2.2	0.5	0.35	0.13	0.08
			1.5	3	1.2	0.31	0.07	0.06
			1	3.5	1	0.34	0.08	0.04
			1.4	2	0.04	0.26		
			0.8	2	1	0.26		
		7	0.8	1.5	0	0.25		
			1	1.5	0	0.35	0.05	0.04
			1.5	2	0.2	0.35	0.09	0.07
			0.8	2	0.6	0.31		
			1	2	0.5	0.29	0.08	0.04
		8	1.8	1.5	0.9	0.29	0.1	0.07
			1.9	1.3	1.2	0.36	0.12	0.1
			1.7	1.7	0	0.41	0.09	0.09
			1.2	1.5	0.2	0.37	0.09	0.07
			0.5	1.2	0.3	0.56	0.07	0.06
		9	1.8	2.2	0.5	0.45	0.1	0.09
			1.2	1.5	0.3	0.43	0.07	0.05
			2.6	3.8	1.4	0.37	0.17	0.13
			1.2	1.2	0	0.31	0.09	0.07
			1.1	1.1	0.2	0.41	0.05	0.04
		10	1.2	2.2	1.5	0.31	0.08	0.06
			1.4	2.3	0.4	0.31	0.06	0.04
			2.8	3.5	0.9	0.44	0.21	0.2
			1.7	3.5	2.5	0.36	0.1	0.01
			1.4	2.4	0.3	0.3	0.07	0.06
		11	1.3	3.2	0.7	0.45	0.11	0.09
			0.9	2.6	0.3	0.37	0.09	0.07
			2.1	2.7	3.1	0.45	0.14	0.13
			1.4	2.7	0.6	0.38	0.1	0.07
			2.4	2.4	1.3	0.44	0.16	0.14
		12	2.5	2.5	1	0.34	0.18	0.12
			2.2	3	2.2	0.34	0.14	0.1
			1.4	2.5	0.5	0.33	0.07	0.06
			0.9	1.1	0	0.24		
			1.5	2	1	0.31	0.07	0.07

Section	Date	Plot	Shoot (cm)	Root (cm)	Longest root (cm)	Diameter (cm)	Weight (g)	Weight shoot (g)
G	**01-07**	**7**	5.4	7.9	1	0.5	0.83	0.74
			4.5	8.2	2	0.6	2.01	1.84
			9.5	4.7	2.8	0.61	1.84	0.74
			7.6	5.6	1.5	0.58	1.08	0.99
			7.3	5.1	1	0.46	0.68	0.66
		8	8.6	6	2.1	0.65	1.97	0.173
			7.6	4.6	1.5	0.45	0.93	0.86
			10	6.7	1.5	0.55	2.07	1.87
			13	5.4	2	0.45	2.19	1.9
			12.9	8.4	3.2	0.5	3.37	2.64
		9	8.6	3		0.45	0.78	0.71
			9.1	4	2.5	0.46	0.94	0.72
			5.1	3.9	1.5	0.36	0.29	0.27
			11.2	5.9	0.5	0.42	1.23	1.07
			10.5	9	3	0.55	1.78	1.35
		10	7.4	7.8	1.5	0.4	0.63	0.61
			5.3	5	0.5	0.38	0.43	0.41
			6	3		0.36	0.38	0.36
			7.4	9.4		0.38	0.87	0.71
			4.2	6.9		0.38	0.34	0.31
		11	5.2	7.1	2	0.5	1.29	1.09
			7.8	6.1	0.3	0.45	0.75	0.64
			6.7	7		0.37	0.59	0.55
			6.4	7.2	1	0.42	0.57	0.48
			6	4		0.4	0.49	0.38
		12	6.4	7.7	3.7	0.34	0.44	0.42
			8.9	9	2.1	0.36	0.98	0.86
			7.4	6.4		0.36	0.5	0.45
			10.2	11.5	1.5	0.46	1.68	1.54
			6.5	4.7	0.9	0.56	0.59	0.56

Section	Date	Plot	Shoot (cm)	Root (cm)	Longest root (cm)	Diameter (cm)	Weight (g)	Weight shoot (g)
E	**01-07**	**2**	9.9	4.7	1.3	0.54	1.47	1.13
			10	6.1	1.4	0.5	1.58	1.26
			13	3.5	1.8	0.48	3.23	2.76
			10.2	5.9	1	0.56	1.58	1.42
			11.5	3.4	5	0.56	2.13	1.82
		3	9.5	6.7	3	0.55	4.55	1.25
			6	2.8	0.7	0.41	0.58	0.54
			5.5	2.1	4	0.43	0.58	0.45
			8	3	0.6	0.45	0.64	0.61
			7.3	3.5	0.3	0.42	0.87	0.79
		4	4.5	3.7		0.29	0.18	0.16
			3.2	4.5	2	0.4	0.35	0.32
			7.3	10		0.46	0.69	0.61
			4	5.1		0.44	0.27	0.27
			3.7	5.2		0.34	0.2	0.19
		5	3.5	4.2	2.7	0.38	0.32	0.25
			4	8	4.5	0.37	0.33	0.2
			3.4	3.6	0.6	0.27	0.18	0.16
			4.7	6.7	2.2	0.43	0.38	0.35
			3.9	4.6	2.7	0.43	0.29	0.25
		6	7.2	4.2	0.5	0.42	0.81	0.75
			6.3	3.5		0.36	0.39	0.39
			7.8	3.5	2.5	0.43	0.66	0.52
			6.5	7.2	0.6	0.4	0.69	0.54
			7.5	5	1	0.4	0.61	0.5
		7	9.5	3.7	1	0.48	1.08	0.91
			12	4	1.6	0.44	2.92	2.61
			6.2	2.5	0.5	0.38	0.42	0.4
			8.1	4	1.1	0.36	0.77	0.67
			8	4	0.9	0.43	0.62	0.5
		8	6.7	4	1	0.37	0.7	0.56
			4.5	4.5	2	0.36	0.34	0.26
			9.6	2.7	2.5	0.48	1.19	0.77
			10.9	4	3	0.53	1.51	1.24
			5.6	5.4	0.4	0.43	0.54	0.45
		9	8.8	6.5	1.2	0.67	1.15	0.98
			12	7.5	3	0.67	3.81	3.21
			8.8	4.2	2	0.52	1.3	1.16
			7.4	3.5	0.2	0.52	0.68	0.52
			11.3	4.7	1	0.66	2.17	1.8
		10	4.8	3.5	0.7	0.4	0.44	0.33
			8.4	8.2	3.3	0.48	0.86	1.07
			11.6	4	2.1	0.53	2.54	2.27
			8.6	4.4	2.4	0.56	2.12	1.86
			9.1	5.2	2	0.47	0.8	0.6
		11	10.9	5	2.5	0.6	2.44	1.94
			6.5	5.8	3.3	0.42	0.59	0.45
			8.3	6.1	1.1	0.5	1.14	0.94
			8.5	4	0.9	0.5	1.46	1.28
			5.2	4.2	0.7	0.32	0.35	0.33
		12	6.5	2.4	0.5	0.5	0.71	0.68
			9.4	4.6	1.3	0.45	0.93	0.76
			10.4	4.5	1	0.62	1.69	1.49
			17.1	2	3.6	0.47	3.99	3.63
			7	3.2	1.8	0.3	0.73	0.62

Section	Date	Plot	Shoot (cm)	Root (cm)	Longest root (cm)	Diameter (cm)	Weight (g)	Weight shoot (g)
G	**30-07**	**7**	15	15	12	0.45	5.76	5.09
			23	7	6	0.43	7.33	6.67
			27.5	10.5	8.7	0.6	17.56	15.89
			22.2	18	9.1	0.26	12.13	10.16
			15	5	4	0.46	2.83	2.67
			17.2	8.6	4.6	0.52	3.43	2.64
			17	7.6	4.5	0.4	4.5	4
		8	23.4	11.5	11.2	0.47	9.76	8.93
			11.2	9.8		0.36	1.15	0.92
			18.7	6.1	2.5	0.35	2.84	2.23
			17	10.5	5.1	0.38	3.2	3
			15	8.5	3.2	0.29	1.59	1.46
			17.1	10	8	0.48	3.94	3.57
			15.2	12.6	5.8	0.47	2.55	2.09
		9	19.6	11.6	2.4	0.35	2.81	2.33
			17	7.6		0.35	1.92	1.43
			17	9		0.4	1.78	1.38
			18.5	10	4.5	0.36	3.67	3.41
			16.7	10.5		0.3	1.88	1.48
			15.9	11.2	5	0.4	2.37	1.87
			24.4	17	2	0.46	5.65	4.6
		10	16	13.6	3.3	0.48	3.76	3.55
			13.1	10.4	2.7	0.4	1.4	1.18
			14.7	12.7	6.5	0.45	2.54	2.15
			16.7	9.5	4	0.4	1.97	1.77
			9.4	5.6	1	0.29	0.62	0.48
			15	8	2.5	0.37	4.33	4
			19	13		0.45	2.75	2.39
		11	15.6	13	4	0.5	4.96	4.71
			11	4.5	3	0.38	1.07	0.97
			19.9	11	8.2	0.48	4.16	3.74
			15.1	10	7.4	0.38	1.62	1.43
			13	10.5		0.32	1.85	1.79
			12.5	11	2	0.35	2.18	2.01
			14.5	7.5	6.5	0.45	6.36	5
		12	14	9.7	2.1	0.36	1.72	1.59
			15.9	8.5	2.2	0.43	3.37	3.16
			17	9.7	4	0.35	2.4	2.05
			10.2	5.1	1	0.3	0.83	0.81
			18.8	14	12.3	0.48	4.12	12.3
			14.4	13	6	0.41	3.28	3.09
			19.6	12.5	4.7	0.37	4.06	3.49

Section	Date	Plot	Shoot (cm)	Root (cm)	Longest root (cm)	Diameter (cm)	Weight (g)	Weight shoot (g)
E	**30-07**	**2**	18.5	7.5	6	0.45	8	6.1
			14.5	3.5	2.5	0.32	4.71	4.25
			18.6	6.3	4	0.48	7.38	5.96
			19.9	5.4	3.6	0.43	4.2	3.59
			26	5	3.2	0.48	9.55	5.1
			26.4	6	3	0.47	12.62	9.89
			22	4	4.5	0.36	6.26	3.99
		3	13.9	4.1	5.4	0.41	3.34	2.54
			20	8	6.3	0.52	9.16	6.91
			21	7.4	4.6	0.74	13.71	11.11
			18.5	6.5	3.6	0.5	7.13	4.86
			16.1	6.6	4	0.5	5.7	4.68
		4	7.2	6.4		0.17	0.34	0.22
			5.1	8.2		0.37	0.35	0.28
			6.9	12		0.32	0.6	0.45
			5.5	4.6	0	0.3	0.5	0.39
			5	6	0	0.14	0.93	0.86
			12	14.6	5.1	0.4	2.67	2.18
			11.9	17	6.9	0.41	1.68	1.24
		5	12.7	8	0	0.42	1.16	0.91
			11	8	4	0.3	1.56	1.32
			14.5	7	2.5	0.31	2.7	2.2
			10.3	8.2	0	0.22	0.52	0.43
			20	10	11	0.3	5.39	4.32
			16.2	6.5	5	0.5	4.1	3.5
			17	6.6	3.5	0.47	3.06	2.43
		6	17	6	2	0.38	2.04	1.31
			18.2	3.5	4	0.48	2.67	1.76
			19.5	4	4	0.35	2.52	1.76
			19.2	7	6	0.55	5.42	3.5
			15.1	7	4	0.31	1.61	1.21
			11.7	7	1.2	0.47	1.76	1.26
			14.4	5.6	1.2	0.38	2.76	1.53
		7	25	4.5	3	0.41	6.75	5.46
			21	3	2	0.43	4.84	3.65
			20.5	4	3.9	0.45	3.96	2.9
			19.5	4	1.5	0.41	1.91	1.44
			29	3		0.35	19.56	7.93
			20.3	6.7	2.5	0.53	3.55	2.95
			24.5	2	1.6	0.55	4.01	3.04
		8	12.7	2.6	1.5	0.35	2.29	1.81
			23.7	5.5	5.4	0.31	9	7.72
			15.2	6.5	6	0.22	2.62	1.97
			19.5	4.5	2.3	0.5	4.69	3.99
			24.9	6	5.9	0.27	6.95	4.49
			11.6	6	2.5	0.33	1.01	0.83
			13.5	7	2.2	0.48	1.39	1.06
		9	15.6	9	5.2	0.5	3.57	2.92
			19	6	1.8	0.51	2.67	2.18
			19	6.7	2.5	0.36	5.35	4.6
			15	4.6	1.3	0.36	2.23	2
			12.6	7.6		0.31	1.06	0.95
			17.6	10.4	5.2	0.5	6.18	4.54
			9.5	12.4	2.6	0.35	2.16	1.59
		10	13	6.2	2.6	0.48	1.75	1.38
			18.6	5.6	3.4	0.46	4.01	3.15
			18	4.9	4.6	0.45	4.3	3.41
			15	6.2	1	0.44	1.5	1.27
			17.6	6.2	6	0.27	6.82	5.35
			19	8.7	4.5	0.37	3.52	2.62
			18.6	8	4.5	0.5	7.13	5.22
		11	18	5.5	5	0.44	3.31	2.48
			14.8	5	1	0.35	2.18	1.76
			16.4	4.4	2.1	0.48	3.48	3.05
			19.2	5.8	2.5	0.35	6.77	5.85
			12.7	2.5	2.5	0.36	2.08	1.65
			18	9.6	5.5	0.4	6.82	4.75
			13	4.5	2.7	0.34	1.31	1.04
		12	20.6	4	3.1	0.4	3.76	3.15
			18.6	2.5	4	0.4	1.97	1.39
			11.6	4.2		0.36	1.06	0.98
			14.4	4.9	2.7	0.35	1.16	0.85
			22.5	5.5	2	0.43	4.6	3.8
			19.6	6.2	6.2	0.5	4.79	3.43
			14.6	3	3.5	0.43	2.41	2.05

Section	Date	Plot	Shoot (cm)	Root (cm)	Longest root (cm)	Diameter (cm)	Weight (g)	Weight shoot (g)
G	**28-09**	**7**	24.2	12	4.6	0.22	5.15	4.65
			15.1	13.1	7.6	0.22	2.82	2.3
			25	8.5	2.5	0.27	9.17	8.63
			16.8	6.1	1.2		1.92	1.79
			22.1	10.2	3	0.21	7.83	7.18
		8	28.1	5.6	4.1	0.35	14.48	12.12
			17.1	14.7	4.2	0.18	2.89	2.36
			26.2	11.5	2.1	0.22	6.39	5.63
			21.8	12.9	6.6	0.34	13.65	13.07
			27.2	14.5	9.9	0.4	16.7	14.57
		9	21.8	4.1	2.4	0.2	3.21	2.71
			20.2	6.4	6.7		1.58	1.43
			22.5	7.2	3.5	0.24	3.37	2.83
			22.5	9.6	1.2	0.21	1.9	1.64
			23	9.7	2.1	0.32	5.38	4.63
		10	19.5	10.5	6.5	0.22	4.23	3.94
			22.6	13.7	4.3	0.22	4.01	3.51
			11.5	10.2	1.5		1.2	1.18
			12.5	3.2			0.74	0.62
			12.1	7.1			0.86	0.77
		11	18.2	9.5	3.1	0.17	2.45	2.21
			17.8	7.4	1.8	0.22	2.5	2.13
			18.7	11	2.1	0.22	1.61	1.25
			14	6.6	4.1		2	1.82
			9.7	6.9	1		1.27	1.07
		12	16.1	8.9	2.9		1.65	1.48
			18.5	8.7	1.6	0.21	2.4	2.16
			15.5	9.5	2.2		1.5	1.38
			21.8	7.6	5.1	0.27	5.71	3.93
			17	5.5	6.5	0.2	3.83	3.1

Section	Date	Plot	Shoot (cm)	Root (cm)	Longest root (cm)	Diameter (cm)	Weight (g)	Weight shoot (g)
E	**28-09**	**2**	26.4	5.9	4	0.46	8.38	6.44
			19.7	3.9	2.5	0.36	3.09	2.59
			26.1	6	2	0.54	14.18	9.89
			23	2.9	1.5	0.35	4.06	3.71
			24.6	3.6	2.6	0.55	12.17	7.83
		3	22	5.2	7	0.35	9.85	8.51
			24	5.2	3.1	0.48	15.39	12.72
			27.7	8.1	3.7	0.37	11.82	10.43
			19	8.1	6.9	0.4	11.66	9.77
			27.3	4.3	3.1	0.55	10.56	9.52
		4	10	6.6			0.42	0.4
			16.6	7.2			0.68	0.51
			9.2	4.6			0.52	0.49
			11.6	5.9			0.96	0.87
			12.1	6.1			1.27	0.69
		5	17.6	7.9	5.1	0.3	3.06	2.67
			19.5	9.5	11.6	0.37	7.91	6.68
			18.1	10.2	8.5	0.28	6.43	5.35
			19.5	7.5	9.6	0.36	3.58	2.04
			16.9	8	7.6	0.24	5.45	4.84
		6	20.5	3.2	3.1	0.17	2.14	1.89
			27.2	3.1	2	0.3	4.91	3.96
			28.9	5	1.2	0.46	12.26	10.16
			22	3.5	1.7	0.48	7.12	5.7
			27.2	5.5	5	0.46	16.29	14.65
		7	31.5	3.8	6.2	0.52	24.65	21.17
			28.1	6.1	3.1	0.35	8.81	8.21
			29.1	5.6	3.2	0.33	13.04	10.71
			33	5.8	4.9	0.46	11.61	8.39
			24	6	2	0.35	5.14	4.39
		8	20.6	4.5	3.1	0.34	4.95	3.19
			22.6	8	9	0.35	4.01	3.34
			21.2	5.1	2	0.34	1.33	3.63
			23.8	6.1	7.5	0.35	3.57	2.92
			13	3.1			1.08	0.92
		9	14.1	2.9	1.4	0.2	2.44	2.27
			20.2	6.6	2.9	0.35	3.6	3.21
			11.9	3.2			1.56	1.49
			15.2	3.6			1.4	1.25
			11.9	3.5			0.79	0.73
		10	19.6	5.2	3.2	0.45	6.85	5.65
			15.9	5.4	1.1	0.27	2.03	1.75
			20.6	7.6	4.3	0.41	6.14	4.99
			13.5	6	3	0.31	4.54	4.13
			26	9.5	8.6	0.34	5.59	4.24
		11	15.1	5.4	4.1	0.27	4.77	4.46
			28.6	6.1	2	0.4	12.89	11.6
			18.7	6.6	4.5	0.3	4.59	4.26
			19	8	5.5	0.35	6.22	5.36
			26.4	8	5.1	0.5	13.58	11.24
		12	15.6	3.6	2.1		1.36	1.26
			24.7	5.2	6.3	0.38	4.22	3.1
			22.4	6.1	8.4	0.61	18.42	15.88
			21.8	5.5	4.2	0.43	5.85	4.88
			20.1	5.1	3.2	0.23	3.22	2.86

F Values for FVC

Values for the vegetation cover of each separate vegetation plot during the field trips. The final field trip in September is not included, since the Salicornia have turned red already by that time. The values indicated in red represent untrustworthy values by reasons described in the Discussion. These values have been replaced by the values between the brackets, which are determined on visual clues from the photograph.

Section	Plot	Date		
		02-06	01-07	30-07
E	**1**	0	0	0
	2	30.14 (2)	17.45	62.91
	3	5.18 (1)	9.44	5.25
	4	0.4	5.33	2.78
	5	0.74	2.27	3.86
	6	66.12 (5)	6.41	76.12 (8)
	7	7.41 (4)	19.75	43.5
	8	0.76	1.81	5.11
	9	1.41	8.99	9.35
	10	0.074	4.6	4.68
	11	0.38	1.87	11.38 (7)
	12	3.35	15.39	28.98
G	**1**	0	0	0
	2	0	0	0
	3	0	0	0
	4	0	0	0
	5	0	0	0
	6	0	0	0
	7	0.2	8.5 (1)	24.3 (5)
	8	0.51	7.08	10.67
	9	1.36	10.37	22.52
	10	0.02	3	4.18
	11	0.36	3.57	5.27
	12	0.45	6.53	8.6

G Total sedimentation under different dam heights

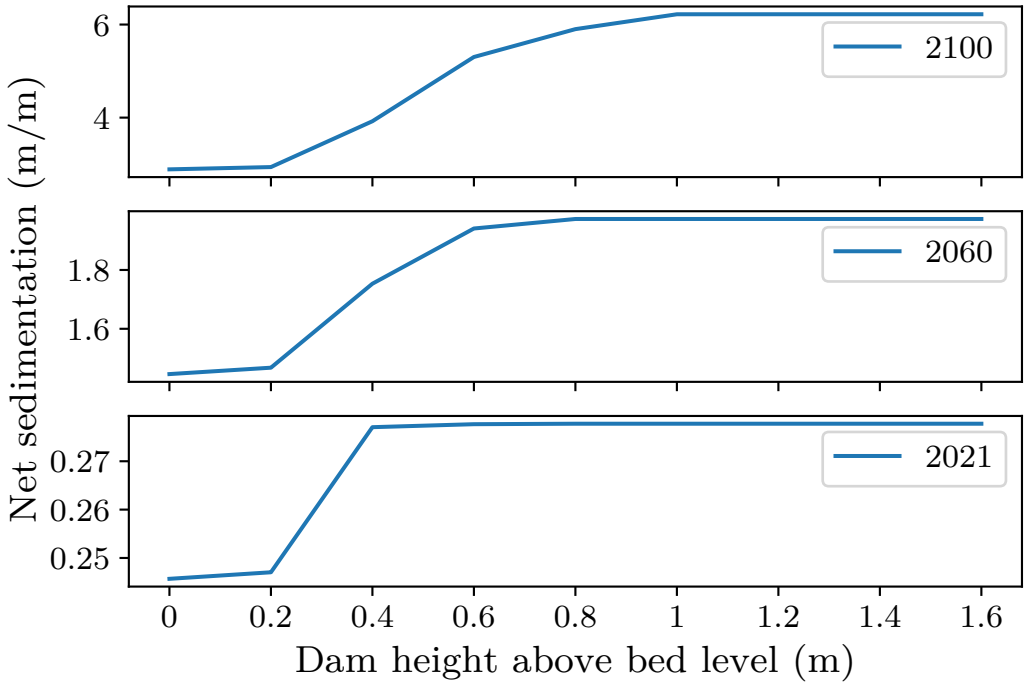

Net sedimentation that occurred landward of the dam over the simulation of one growing season during the years 2021, 2060, and 2100 with different dam heights ranging from no dam (0) to a dam with a height of 1.6 m above the bed. An increase in accretion is visible until different dam heights above the bed for the different scenarios: 0.4, 0.8, and 1 m for the years 2021, 2060, and 2100 respectively.

H Calibration of section G

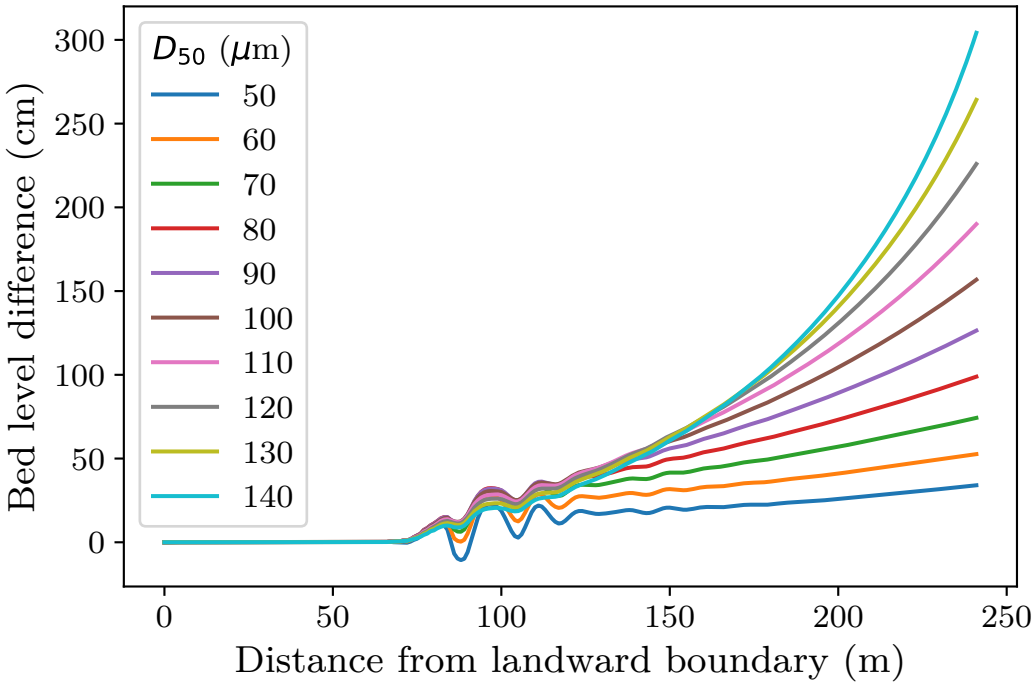

Difference between the initial bathymetry of section G and the bathymetry after the simulated growing season with different sediment characteristics. Positive values represent sedimentation and negative values represent erosion.